Sheffield Hallam University

Complex kame belt morphology, stratigraphy and architecture

LOVELL, Harold, LIVINGSTONE, Stephen, BOSTON, Clare, BOOTH, Adam, STORRAR, Robert <http://orcid.org/0000-0003-4738-0082> and BARR, Lestyn

Available from Sheffield Hallam University Research Archive (SHURA) at:

http://shura.shu.ac.uk/24768/

Published version

Copyright and re-use policy

Complex kame belt morphology, stratigraphy and architecture

Harold Lovell[1*], Stephen J. Livingstone[2], Clare M. Boston[1], Adam D. Booth[3], Robert D. Storrar[4] and Iestyn D. Barr[5]

[1]Department of Geography, University of Portsmouth, Portsmouth, PO1 3HE;

[2]Department of Geography, University of Sheffield, Sheffield, S10 2TN;

[3]School of Earth and Environment, University of Leeds, Leeds, LS2 9JT

[4]Department of the Natural and Built Environment, Sheffield Hallam University, Sheffield, S1 1WB

[5]School of Science and the Environment, Manchester Metropolitan University, Manchester, M15 6BH

*Correspondence: harold.lovell@port.ac.uk

Abstract

The development of glacier karst at the margins of melting ice sheets produces complex glaciofluvial sediment-landform assemblages that provide information on ice sheet downwasting processes. We present the first combined geomorphological, sedimentological and geophysical investigation of the Brampton Kame Belt, an important glaciofluvial depositional zone at the centre of the last British-Irish Ice Sheet. Ground-penetrating radar (GPR) data allow the broad scale internal architecture of ridges (eskers) and flat-topped hills (ice-walled lake plains) to be determined at four sites. In combination with sediment exposures, these provide information on lateral and vertical variations in accretion styles, depositional boundaries, and grain size changes. Building on existing work on the subject, we propose a refined model for the formation of ice-walled lake plains resulting from the evolution and collapse of major drainage axes into lakes as stable glacier karst develops during deglaciation. The internal structure of esker ridges demonstrates variations in sedimentation that can be linked to differences in ridge morphologies across the kame belt. This includes low energy flow conditions and multiple accretion phases identified within large S-N

1

oriented esker ridges; and fluctuating water pressures, hyperconcentrated flows, and significant deformation within a fragmented SW-NE oriented esker ridge. In combination with updated geomorphological mapping, this work allows us to identify two main styles of drainage within the kame belt: (1) major drainage axes aligned broadly S-N that extend through the entire kame belt and collapsed into a chain of ice-walled lakes; and (2) a series of smaller, fragmented SW-NE aligned esker ridges that represent ice-marginal drainage as the ice sheet receded south-eastwards up the Vale of Eden. Our study demonstrates the importance of integrated geomorphological, sedimentological and geophysical investigations in order to understand complex and polyphase glaciofluvial sediment-landform assemblages.

Key words: Kame, glaciofluvial, geomorphology, sedimentology, ground-penetrating radar (GPR), British-Irish Ice Sheet

Introduction

Ice sheet downwasting and recession leads to the deposition of large zones of ice-contact glaciofluvial and glaciolacustrine sediment-landform assemblages. These assemblages are often given the general term 'kames' or 'kame belts' and are formed where sediment and meltwater accumulates in interlobate locations and/or areas constrained by local or regional topography (Curtis and Woodworth, 1899; Flint, 1928a,b, 1929; Cook, 1946; Holmes, 1947; Winters, 1961; Rieck, 1979; Warren and Ashley, 1994; Thomas and Montague, 1997; Mäkinen, 2003; Livingstone et al., 2010a; Evans et al., 2017). Kame belts are characterised by large volumes of sands and gravels and a complex geomorphology of ridges, mounds, flat-topped hills,

2

depressions, and meltwater channels (Woodworth, 1894; Cook, 1946; Holmes, 1947; Winters, 1961; Huddart, 1981; Malmberg Persson, 1991; Auton, 1992; Attig and Clayton, 1993; Thomas and Montague, 1997; Johnson and Clayton, 2003; Livingstone et al., 2010a; Schaetzl et al., 2013; Attig and Rawling III, 2018). The complex sediment-landform assemblage originates from the development of a glacier karst system formed by extensive supra-, en- and subglacial channel networks and supraglacial ponding, fed by increased meltwater production during ice sheet recession (Clayton, 1964; Price, 1969; Huddart, 1981; Brodzikowski and van Loon, 1991; Bennett and Evans, 2012). Understanding the genesis of the various elements that comprise complex kame topography is crucial to reconstructing ice-marginal and interlobate environments, and deciphering the pattern, style and pace of deglaciation and ice sheet wastage (Warren and Ashley, 1994; Thomas and Montague, 1997; Livingstone et al., 2010a).

The Brampton Kame Belt is located in the central sector of the last (Late Devensian) British-Irish Ice Sheet (Fig. 1). At ~44 km^2, it is one of the largest areas of glaciofluvial sediment deposition in the UK (Livingstone et al., 2008). The kame belt formed between the Penrith sandstone outcrop and north Pennine escarpment during deglaciation as the Tyne Gap Ice Stream receded westwards across the Solway Lowlands and Vale of Eden ice receded south-eastwards (Trotter, 1929; Huddart, 1981; Livingstone et al., 2010a,b, 2015). A minimum age of 15.7 ± 0.1 cal. ka BP for deglaciation of the kame belt was presented by Livingstone et al. (2015), based on radiocarbon dating of organic sediment in a core taken from the Talkin Tarn kettle lake (Fig. 2A). The kame belt comprises a series of ridges, mounds, flat-topped hills, and depressions (Trotter, 1929; Huddart, 1981; Livingstone et al., 2010a), and is the downstream extension of a series of subglacial and lateral meltwater channels

extending SE-NW along the lower slopes of the Pennine escarpment (Trotter, 1929; Arthurton and Wadge, 1981; Greenwood et al., 2007; Livingstone et al., 2008). Aided by insights into the sedimentary composition provided by borehole records and sections in sand and gravel quarries, Huddart (1981) and Livingstone et al. (2010a) interpreted the ridges as eskers originating from sub-, en- and supraglacial meltwater channels; the flat-topped hills as ice-walled lake plains; and the depressions as kettles. Formation during deglaciation was time-transgressive, with polyphase and polygenetic landform and sediment deposition controlled by the evolution of an enlarging glacier karst, and by extensive reworking and fragmentation during topographic inversion (Livingstone et al., 2010a).

The widespread availability of high-resolution digital elevation models (DEMs) has enabled the complex topography of some kame deposits to be mapped in detail (e.g. Livingstone et al., 2010a; Schaetzl et al., 2017). However, establishing process-form relationships for the range of different landforms based on their internal sediments is more challenging, given the sparse distribution and single point nature of sedimentological data. A number of studies have instead conducted geophysical investigations using ground-penetrating radar (GPR) to provide information on subsurface sedimentary architecture in glacial environments (Woodward and Burke, 2007), often where suitable sediment exposures are limited or absent (e.g. Busby and Merritt, 1999; Cassidy et al., 2003; Sadura et al., 2006; Lukas and Sass, 2011; Pellicer and Gibson, 2011; Spagnolo et al., 2014).

In this study, we use GPR and sedimentological data to investigate the sedimentary architecture of the Brampton Kame Belt. The information on internal structure is combined with updated mapping from a high-resolution DEM to provide a

new appraisal of the kame belt and refine existing models for the formation of complex glaciofluvial assemblages.

Methods

Geomorphological mapping

Mapping was conducted within a GIS on hillshaded DEMs following the suggestions of best practice outlined in Chandler et al. (2018). Two mosaiced DEMs were used: a 1 m resolution digital surface model (DSM) provided by the Environment Agency from airborne LiDAR data (available via environment.data.gov.uk/ds/survey), and a 5 m resolution NEXTMap DSM provided by the British Geological Survey for NERC from airborne Interferometric Synthetic Aperture data (available via ceda.ac.uk). The 1 m DSM was used for the majority of the mapping, with the 5 m DSM providing coverage for a small strip missing from the 1 m DSM. Similar to Livingstone et al. (2010a), mapping focused on the identification of key landforms based on morphological characteristics: ridges and mounds (mapped as polygons) with ridge crest lines (mapped as lines); flat-topped hills (polygons); depressions (polygons); and channels (lines).

Sedimentology

Sedimentological investigations, where possible, were used in conjunction with the GPR data to inform the interpretation of radar profiles. Two pre-existing sediment exposures within small quarries at the Morley Farm and Brampton Farm sites (Fig. 2B) were logged in the field as scaled section sketches. Grain size, sedimentary structure,

bedding contacts, and evidence for deformation were recorded at each site. Sedimentary units were identified using the lithofacies codes of Evans and Benn (2004). Structural measurements (strike/dip) were taken to characterise the trend of bedding and faults. Additional sedimentological data presented by Livingstone et al. (2010a), based on sediment exposures in quarries and a number of borehole logs, provided further insight into the wider sedimentary composition and stratigraphy of the kame belt.

GPR data acquisition and processing

GPR survey lines were collected using a Mala 100 MHz unshielded Rough Terrain Antenna (RTA). Survey lines were collected at an even walking pace, with traces collected every 0.25 s and stacked automatically using the autostacks setting. The topography and length of survey lines were recorded simultaneously using a TopCon differential GPS. An effort was made to avoid objects (e.g. trees, fences, walls) that could introduce noise to the surveys, although this was often unavoidable towards the start and end of lines due to the constraints of working in fields. GPR data processing was conducted in Sandmeier ReflexW software, with trace interpolations and topographic corrections performed in Mathworks MATLAB software. All profiles followed the same generic processing sequence. Prior to interpolation, spurious frequency content in the profiles was removed using dewow and bandpass filters, with frequencies outside of the bandwidth 40-120 MHz suppressed. Trace first-breaks were then corrected to 6.7 ns, the travel-time of the direct airwave across the 2 m transmitter-receiver offset in the 100 MHz RTA, before profiles were exported to MATLAB. Since trace acquisition in the profiles was triggered at a fixed time interval,

the distance interval between traces depends on the tow speed and can vary along and between profiles. It must therefore be regularised before any spatial processing step (e.g. migration) can be applied. In raw data, excluding static traces, the mean trace interval is 0.29 ± 0.05 m. A 2D linear interpolation algorithm was applied to regularise the trace interval to 0.25 m, with the time sampling interval also interpolated from the raw value of 0.9674 ns to a more convenient 1 ns. Regularised data were reimported to ReflexW for Kirchhoff migration, which assumed a velocity of 0.12 m/ns (measured from sparse diffraction hyperbolae in the record, given the inability to perform common midpoint surveys with the RTA) and an aperture of 12 m. Horizontal striping was suppressed using a 2D subtracting-average filter, spanning a 4 m trace range, and amplitudes were boosted using a 75 ns automatic gain control window. Depth conversion and topographic corrections were applied to the migrated data in MATLAB, again assuming a velocity of 0.12 m/ns, with the reference datum being the highest elevation point in the profile (or in the group of intersecting profiles). Finally, fully-processed profiles were imported into Schlumberger Petrel software for visualisation.

Results and interpretation

Geomorphology

We mapped over 400 ridges and mounds across the Brampton Kame Belt (Fig. 2), substantially adding to the original mapping of Livingstone et al. (2010a). Ridges display a wide range of morphologies, dimensions and orientations. We also mapped a number of rounded mounds with no discernible crest lines or orientation. The largest ridge is the Brampton ridge in the north of the kame belt (BR in Fig. 2B), which is

straight, single-crested, ~3 km long, ~300 m wide and reaches a height of ~50 m above the surrounding terrain. Several other ridges are up to ~2 km in length, but the majority are shorter (mean ridge crest length = 227 m, n = 439) and <20 m high. Ridge morphology ranges from straight to sinuous. Ridges are generally single-crested, but there are some notable multi-branched morphologies (e.g. the large ridge at Carlatton Farm), and others with multiple crests caused by channel dissection transverse to the main ridge alignment (Fig. 2). Ridge orientation varies across the kame belt. In the south, ridges are generally aligned SE-NW and SW-NE, transitioning to S-N in the central part of the kame belt. Towards the north, the ridges return to a SW-NE alignment leading to W-E where the kame belt trends towards the Tyne Gap (Fig. 2B). Ridges are interpreted as eskers originating from sub-, en- and supraglacial channels (e.g. Woodworth, 1894; Flint, 1928b, 1930; Mannerfelt, 1945; Lewis, 1949; Brennand, 1994; Warren and Ashley, 1994; Livingstone et al., 2010a).

Flat-topped hills are raised features reaching a height of ~20 m above the surrounding terrain, with clearly identifiable flat upper surfaces. The largest flat-topped hills are ~1 km wide and are generally grouped together in a ~2 km wide, 7 km long zone in the central part of the kame belt (Fig. 2B). Esker ridges are closely associated with flat-topped hills in a number of places. In some instances, ridges transition into flat-topped hills and appear to be partially buried by them (e.g. immediately south of North Scales); elsewhere ridges are superimposed on the surface of flat-topped hills. Flat-topped hills are interpreted as ice-walled lake plains (e.g. Cook, 1946; Winters, 1961; Clayton, 1967; Clayton and Cherry, 1967; Huddart, 1981; Clayton et al., 2001, 2008; Johnson and Clayton, 2003; Livingstone et al., 2010a; Curry and Petras, 2011; Stanley and Schaetzl, 2011).

Depressions are distributed throughout the kame belt (Fig. 2B), ranging in size from Talkin Tarn (~500 m wide, ~700 m long) to small (<20 m wide), circular depressions. The densest cluster of depressions is in the southern and central part of the kame belt, giving a pockmarked appearance to the terrain (Livingstone et al., 2010a). Depressions are often located between closely-spaced esker ridges and, in places, cut into them (Fig. 2B). The majority (72%) of the depressions are dry, with only 12 containing water at the time they were mapped. The depressions are interpreted as kettles (e.g. Trotter, 1929; Maizels, 1977; Livingstone et al., 2010a). Whether a kettle is currently dry or is water-filled is likely controlled by its position relative to the water table and the connectivity to the groundwater system (e.g. Cook, 1946; Gerke et al., 2010; Levy et al., 2015; Lischeid et al., 2017; Kayler et al., 2018).

The kame belt contains several channels, ranging from continuous channels that form part of an extended regional meltwater system, to shorter channel fragments (Fig. 2B). A parallel series of SE-NW aligned channels that enter the kame belt at its south-eastern edge form part of a major meltwater system that extends for ~50 km along the western flank of the Pennine escarpment (Trotter, 1929; Arthurton and Wadge, 1981; Greenwood et al., 2007; Livingstone et al., 2008, 2010a). Meltwater channels within the kame belt are typically shorter than those outside its limits, and are often routed around the edges of, or between, closely-spaced landforms. In several places, meltwater channels dissect landforms (e.g. a large esker ridge immediately west of Talkin Tarn, and an ice-walled lake plain ~2 km to the south-west of this ridge) (Fig. 2B). The drainage direction of meltwater channels within the kame belt is variable.

Sedimentology and GPR lines

We investigated two sediment exposures and collected seven GPR survey lines totalling ~2 km from esker ridges and ice-walled lake plains at four sites located in the south of the kame belt (Figs. 2B and 3). Intersecting lines were collected across landforms (e.g. parallel and perpendicular to ridge crest lines) at two sites in order to provide an insight into their 3D architecture (Fig. 3). Seven common radar facies (RF1-RF7) were identified from the profiles (Fig. 4). Where possible, these have been interpreted based on the two sites where GPR lines were acquired immediately above logged sediment sections to provide a tie between sediment and radar facies. These interpretations have then been used to guide the analysis of sites with only GPR data.

Morley Farm

The Morley Farm section (Fig. 5) is located in the south-west of the kame belt within a small quarry excavated into the south-west end of a S-N oriented esker ridge. The ridge forms part of a discontinuous series of four ridges interspersed with small depressions (Figs. 2, 3A and 5C). The ~8 m high ridge that the section is excavated into is relatively straight, ~500 m long, and ~150 m wide at its widest, narrowing significantly at its northern end to <30 m. The section is ~12 m long and comprises up to 6 m of gently dipping to horizontal beds of sand (Sh, Sm, Sp) and some fine gravel (GRm). This includes sequences of horizontally laminated and massive fine to coarse sand, with occasional cross-stratification, fining upwards and outsized gravel clasts. Beds are <0.5 m thick and form gently inclined troughs and crests, widening slightly towards the trough bottom and thinning towards the crest. In general, the bedding surfaces appear laterally continuous. Towards the centre of the exposure, bedding within an onlapping trough truncates the underlying bed. The entire section is overprinted by a series of cross-cutting sand-filled veins that bifurcate in a downwards

direction. Differential weathering indicates that the veins are composed of finer sediments compared to the surrounding beds. At the macro-scale, these in-filled veins do not appear to displace the surrounding bedding. Some of the veins can be traced all the way through the section, but the majority are more discontinuous. The cross-cutting veins are most common in the lower beds, and the veins become more parallel in the upper part of the section.

The fine- to coarse-grained sandy lithofacies at Morley Farm indicate deposition in a low energy fluvial environment characterised by variations in flow velocity. The dominance of horizontally laminated sand records planar bed flow in lower and/or upper flow regimes (Miall, 1977, 1985; Allen, 1984), with rarer periods of dune migration recorded by tabular cross-beds. Massive fine-coarse sand beds record suspension settling or high sediment concentration density underflows (e.g. Rust and Romanelli, 1975; Paterson and Cheel, 1997). Granule gravel beds indicate higher energy flows, while truncation of the larger-scale onlapping troughs may be associated with channel migration over time (Gorrell and Shaw, 1991). The cross-cutting veins are interpreted as a conjugate set of sand-filled fractures (Lee et al., 2015). The pervasiveness of the fractures throughout the section, and their cross-cutting relationship with the horizontal to cross-laminated sand beds, indicates that formation of these fractures post-date deposition of the sand beds. Such fracture sets can be formed by hydrofracturing, or by vertical compression, perhaps due to either loading of ice or simply the overlying weight of a thick sediment sequence. In the case of vertical compression, the extensional fractures create a void space that can then be exploited by water escape in the form of liquefaction and injection of sediments to produce the sand-filled fractures (Lee et al., 2015).

GPR line 188 (Fig. 5D) was collected from above the Morley Farm section (with ~2-5 m offset) and extends for 150 m across the full width of the ridge (Fig. 5C). The first ~10-12 m of the line, which coincides with the sediment section, contains strong sub-horizontal reflectors (RF1 in Fig. 5D), and similar reflectors are found in several places across the profile, including beneath the ridge crest at ~50 m and on the south-eastern flank (Fig. 5D). We interpret these as bedded sands, based on the similar sub-horizontal layering of the reflectors and the sands exposed in the section. A series of trough-shaped reflectors can also be identified across the profile (e.g. RF6 in Fig. 5D). These are of a similar scale (~5-10 m across) to the shallow trough seen in the sediment section (Fig. 5B), suggesting a common origin relating to continued sedimentation within a migrating channel system. We note that these features are also similar to channel fills identified in GPR profiles by other studies (e.g. Russell et al., 2001; Winsemann et al., 2018). Sub-horizontal reflectors towards the top of the ridge crest have a more discontinuous, in places disorganised, arrangement (e.g. RF2 in Fig. 5D). This implies that the top of the esker ridge is composed of sediment of a different texture, such as gravel layers (see also similar packages associated with gravels at Brampton Farm, below and Fig. 6). It is also possible that the disorganised reflectors are evidence for deformed sediment packages (e.g. Fiore et al., 2002).

Brampton Farm

The Brampton Farm section (Fig. 6A) is located within a small quarry excavated into the southern flank of a ~10 m high double-branched esker ridge in the south-east of the kame belt (Figs. 2 and 3A). The western end of the section is located at the point where the ridge bifurcates, with the section aligned sub-parallel to the W-E oriented

crest line of the southern branch and extending for ~70 m along its total length of ~150 m (Fig. 6B). The northern branch of the ridge is aligned SW-NE for the first ~100 m after the bifurcation, before curving to the east to become parallel to the southern branch. To the north of the branched ridge there are four parallel S-N aligned esker ridges (Fig. 3B), which mark the start of a discontinuous series of similarly oriented ridges that can be traced for ~4 km into the central part of the kame belt (Fig. 2B). The sediment section (Fig. 6A) comprises a thick (up to 10 m), heavily deformed sequence of interbedded rippled (type-A and -B) and sub-horizontally laminated sands (Sr, Sh), and massive to crudely-bedded clast and matrix-supported gravels (Gm, Gms, Gh). The sands contain frequent interbeds of granule gravel to pebbles (often one clast thick). The western end of the exposure has the greatest thickness of sands (>8 m), with the succession comprising steeply dipping (34°) bedded sands trending towards the south, unconformably overlain by gently dipping sands trending eastwards. The top of the section is incised by a ~5 m wide channel fill of trough-stratified sands and gravel. Tabular sheets, up to several metres thick, of crudely stratified to massive matrix- and clast-supported gravels ranging in size from cobbles to granule gravel and with sharp or erosional lower contacts become more prevalent towards the central and eastern ends of the section. There are occasional imbricated clast clusters, while stratification is imparted by the crude alignment of clasts and variations in matrix concentration and clast size. The gravels contain frequent deformed soft-sediment rafts (Sd) of massive and bedded sand. Clast forms are predominantly rounded to sub-rounded and comprise a mix of lithologies, including Borrowdale Volcanic lavas and Permo-Triassic sandstone. Deformation is pervasive, with the most extensive evidence along the western side (Fig. 6A-C). This includes widespread normal faulting with dips towards the north-east and south, convolute bedding, open fold structures

and clastic dykes. The largest clastic dyke is up to 1 m wide, cuts through the upper gravel bed at the eastern end of the exposure and comprises vertically-aligned laminated fine sand/silt (Fig. 6F). The dyke has deformed edges, tapers slightly downwards and has a sub-horizontal offshoot extending diagonally upwards off the main body.

Alternating gravels and sands at Brampton Farm sediment section record a dynamic fluvial environment, characterised by significant fluctuations in flow velocity and sediment supply (e.g. Banerjee and MacDonald, 1975; Ringrose, 1982; Brennand, 1994). Low energy conditions are recorded by ripples deposited in the lower flow regime (Jopling and Walker, 1968) and laminated sands that demonstrate planar bed flow in lower and/or upper flow regime conditions (Flint, 1930; Miall, 1977, 1985; Allen, 1984). The general trend of palaeocurrent directions revealed by the ripples suggest that water flow was northwards. The gravels are interpreted to have been deposited by powerful fluidal flows, with traction transport dominating where gravels are imbricated, crudely stratified, and clast supported (Brennand, 1994). The crude stratification, reflecting subtle sorting, is likely imparted by pulses in flow strength (Mäkinen, 2003). Isolated patches of openwork gravels likely represent winnowing of finer-grained material (Lundqvist, 1979; Shulmeister, 1989), whereas matrix-supported massive gravels indicate hyperconcentrated flood flow deposits (Saunderson, 1977; Shulmeister, 1989). Further evidence for high energy flows is provided by the soft-sediment rafts, ripped up from underlying beds or derived from bank collapses. The entire section has been heavily deformed, with the prevalence of normal faulting indicative of gravitational failure, possibly due to the removal of supporting ice walls (e.g. Flint, 1930; McDonald and Shilts, 1975; Brennand, 2000; Fiore et al., 2002), and (sub-)vertical clastic dykes (Fig. 6F) recording hydrofracture

14

during periods of high water content and hydrostatic pressure (e.g. Rijsdijk et al., 1999; van der Meer et al., 2009; Phillips and Hughes, 2014).

GPR line 195 (Fig. 6G) is 90 m long and was collected above and adjacent (with ~2-5 m offset) to the Brampton Farm section, which provides an exposure for ~75 m of the GPR line (Fig. 6B). This large overlap allows a number of features to be tied between the section and the radar data. The lower part of the profile, particularly in the central and eastern end (Fig. 6G), is largely composed of strong sub-horizontal reflectors (RF1), interpreted as bedded sands. These areas are consistent with the horizontally bedded sands (Sh, Sr) seen in the sediment section (Fig. 6A) and at Morley Farm (Fig. 5). Gently dipping reflectors in the centre of the profile (RF3) downlap onto well-defined, continuous sub-horizontal reflectors of RF1, consistent with the dip of the bedded sand (Sh) layer seen in the section to the west of the area of slumping. Fainter, more-discontinuous sub-horizontal reflectors (RF2) overlaying RF1 correspond closely to gravel layers (Gh, Gm) seen in the centre and eastern end of the section, suggesting these are sub-horizontally deposited gravel sheets (Fig. 6G). The western end of the sediment section is deformed, with a number of faults visible (Figs. 6A and 6D). The GPR profile in this area of faulting contains several linear features that appear to offset layered reflectors, but these could be radar artefacts rather than the imaging of faults by the radar data. No features matching the hydrofracture at the eastern end of the sediment section (Figs. 6A and 6F) could be identified from the GPR profile.

Carlatton Farm

Two intersecting GPR lines were acquired from close to the crest line of a 1000 m long, 250 m wide, ~12 m high S-N orientated multi-branched esker ridge in the south-

west of the kame belt (Figs. 2B, 3A and 7A). Line 150 (Fig. 7C) is a 140 m long cross profile running perpendicular to (and crossing) the ridge crest line (Figs. 3A, 7A and 7B). Line 155 (Fig. 7D) is a long profile that intersects with line 150 at approximately the ridge crest line before extending ~250 m to the north-west, following a subtle sub-ridge aligned sub-parallel to the main ridge crest line (Figs. 7A and 7B). Areas of strong, quasi-continuous, wavy sub-horizontal reflectors (RF1) are found in the lower part of both profiles. This suggests a ridge core composed of bedded sands (Figs. 7C and 7D), which, coupled with the morphology of the ridge, is indicative of planar flow and vertical accretion in an ice-walled channel. Northwards-dipping reflectors (RF3) at the S end of line 155 suggest downflow accretion of sediments within the esker ridge. Areas of discontinuous sub-horizontal reflectors (e.g. RF2 in Figs. 7C and 7D) may represent deposition of coarser sediment, such as gravel, as seen in the Morley and Brampton Farm profiles (Figs. 5D and 6G). Discontinuous sub-horizontal and wavy reflectors, in places dipping gently southwards, with a hummocky upper surface that mimics the underlying reflectors (RF5), can be identified in line 155. These are consistent with ridge-scale sediment macroforms associated with a dynamic depositional environment (Brennand, 1994; Burke et al., 2015). The dip direction of some reflectors in this zone is opposite to the general northwards drainage trend, indicating that these are shallow backsets related to headward accretion on the stoss-side of the sediment macroform in a channel (e.g. Miall, 1985; Fiore et al., 2002; Heinz and Aigner, 2003; Burke et al., 2008). The transition from northwards dipping reflectors at the southern end of the long profile, to shallow backsets overlying sub-horizontal bedded sands, with a series of clearly defined boundaries, at the northern end, is indicative of multiple phases of accretion and changes in flow conditions within the esker ridge, characterised by significant lateral variation in the radar facies. Line 155

also contains a series of high-angle, disrupted reflectors in the central and uppermost part of the profile (RF7 in Fig. 7D). We interpret this as possible evidence for post-depositional deformation resulting from collapse due to ice melt out/removal of ice walls during deglaciation (e.g. Flint, 1930; Holmes, 1947; McDonald and Shilts, 1975; Brennand, 2000; Fiore et al., 2002; Livingstone et al., 2010a). This is consistent with the geomorphological context, as RF7 is located close to a small (30 m wide) kettle on top of the ridge (Fig. 7A).

North Scales

Three intersecting lines up to 500 m in length were collected across the southern end of a ~20 m high ice-walled lake plain, close to the point where a SW-NE oriented esker ridge meets the hill (Figs. 3A, 8A and 8B). The bottom radar facies in line 159 comprises strong, undulating reflectors with a hummocky surface up to 6 m thick (e.g. RF5 in Fig. 8C). These are overlain by discontinuous dipping reflectors (e.g. RF3 in Fig. 8C) that in places fill troughs in the underlying hummocky surface and tend to thicken from <2 m to >5 m towards the north-west. The RF5 hummocky reflectors (e.g. Fig. 8C, lower panel), also found at Carlatton Farm (Fig. 7D), are consistent with ridge-scale esker macroforms (Brennand, 1994; Burke et al., 2015). The discontinuous dipping reflectors that overlay the hummocky surface are interpreted as foresets (Russell et al., 2001; Woodward and Burke, 2007; Clayton et al., 2008; Winsemann et al., 2018), indicating north-west drainage and sediment progradation into a water body based on the orientation of dip. Sediment infilling of the >5 m deep water body (based on thickness of the foreset structures) has resulted in the formation of the flat-topped surface. Clear downlapping boundaries (RF3 in Fig. 8C) record multiple phases of

accretion and sediment deposition. To the north-west end of the line there are areas of discontinuous, disrupted reflectors (e.g. RF7 in Fig. 8C) that are interpreted as potential evidence of deformation due to removal of lateral ice support leading to sediment collapse (e.g. Holmes, 1947; Fiore et al., 2002; Johnson and Clayton, 2003; Clayton et al., 2008; Burke et al., 2015).

The lowermost radar facies in line 161, which is 5 m thick, consists of strong-sub-horizontal to wavy reflectors (RF1 in Fig. 8D), which are interpreted as vertically-accreted bedded sands (i.e. esker deposits associated with a continuation of the ridge located to the south of the ice-walled lake plain). These are overlain by a series of reflectors dipping to the south-west (RF3 in Fig. 8D) that are restricted to the stoss (south-west) side of the ice-walled lake plain and are up to ~2 m thick, and are in turn overlain by faint, often discontinuous sub-horizontal reflectors with a thickness of ~2 m (RF4 in Fig. 8D). At the north-east end of the profile, the hummocky radar surface (RF5) is draped by discontinuous reflectors that mimic the underlying hummocks (RF4 in Fig. 8D). The draped reflectors are consistent with fine-grained glaciolacustrine sedimentation (topsets) that has buried underlying glaciofluvial deposits. Line 161 also contains a large trough structure at its south-west end (RF6 in Fig. 8D), suggesting the presence of a large channel towards the margin of the ice-walled lake that was buried by subsequent lake infill.

Line 166 contains similar features to those seen in lines 159 and 161. This includes strong sub-horizontal reflectors (e.g. RF1 in Fig. 8E) interpreted as bedded sands laid down as esker deposits; dipping reflectors (RF3 in Fig. 8E) interpreted as foresets and indicating northwards sediment progradation into a lake environment; and an uppermost series of faint sub-horizontal reflectors (e.g. RF4 in Fig. 8E) consistent with deltaic topsets. There appear to be at least two phases of foreset deposition, with

the lowermost foresets contiguous with the bedded sands, followed by a second set of foresets that in places infill the hummocky surface. This suggests formation was characterised by an initial phase of esker formation indicative of vertical accretion (RF1 and RF5), which terminated in a lake forming a subaqueous fan (lower RF3 unit) indicative of more complex horizontal accretion, followed by expansion of the lake, and subsequent infilling and burial of the esker and lower fan by a prograding delta (upper RF3 unit and RF4).

RF3 dipping reflectors are found in all three lines at North Scales and display a range of dip directions from south-west to north. The south-west dipping RF3 reflectors in line 166 contrast to the north-west and north dipping RF3 (interpreted as delta or subaqueous fan foresets) in lines 159 and 166, respectively, and the overall northwards trend of drainage within the kame belt (Huddart, 1981; Livingstone et al., 2010a). There are two possible explanations for this apparent broad range in dip directions. RF3 reflectors in line 161 are consistent with backsets, indicating headward accretion on the stoss-side of the sediment macroform at a hydraulic jump during high-energy water flows (e.g. Fiore et al., 2002; Burke et al., 2008; Winsemann et al., 2018). Alternatively, they could represent foreset deposition in a heavily splayed subaqueous fan/prograding delta, with foreset dip orientation ranging from south-west to north. This would suggest a stream input from the south-east of the ice-walled lake plain. Of these alternatives, we favour the interpretation of RF3 in line 161 as backsets based on their restriction to the stoss side of the ice-walled lake plain, in close proximity to the likely entrance point to the lake of an outflow channel (as indicated by the esker ridge to the south and the evidence for buried esker deposits within the ice-walled lake plain). However, it is also possible that they relate to a large, splayed subaqueous fan feature burying the initial phases of esker sedimentation.

Discussion

Process-form relationships of landforms within complex kame belts

Our interpretation of the North Scales radar data provides a conceptual model for progressive phases of sedimentation during ice-walled lake-plain formation (Fig. 9), building on existing models (e.g. Winters, 1961; Clayton and Cherry, 1967; Johnson and Clayton, 2003; Clayton et al., 2008; Livingstone et al., 2010a,c). The model shows evolution from initial subglacial esker sedimentation to subaqueous fan deposition into a lake following channel collapse and the development of glacier karst (e.g. Flint, 1930; Holmes, 1947; Lewis, 1949; Clayton, 1964; Evans et al., 2018), followed by a final phase of lake and delta infill. The identified radar facies suggest initial glaciofluvial deposition within ice-walled channels, as shown in all three profiles by the lowermost units of bedded sands (RF1) and the ridge-scale hummocky sub-horizontal reflectors (RF5) indicating subglacial esker formation as a series of macroforms (Fig. 8). This glaciofluvial sedimentation is likely to be connected to the ridge located immediately south of the ice-walled lake plain (Fig. 8A). The northwards dipping lower RF3 unit in line 166 is contiguous with the esker sedimentation, suggesting a switch from channel sedimentation to subaqueous fan deposits as the lake begins to form during the initial stages of glacier karst development (Fig. 9C). The south-west dipping reflectors (RF3) in Fig. 8D are likely to be backsets and indicate a high energy hydraulic system consistent with a subglacial channel entering an ice-marginal lake (e.g. Flint, 1930) (Fig. 9D). The backsets are confined to the south and south-west side of the flat-topped hill, closest to the likely input points based on the northwards-draining meltwater system (e.g. Fig. 2B). This sequence suggests higher energy flows to the south-west of the ice-walled lake, transitioning to distal lower energy deposition to the

north-east and the centre of the lake. However, south-west dipping reflectors may alternatively record a heavily-splayed subaqueous fan fed by a stream input at the south-east margin of the lake. Subaqueous fan deposits have been identified in other ice-walled lake plain studies based on the presence of gravelly rim-ridges surrounding the flat-topped hill (e.g. Winters, 1961; Clayton and Cherry, 1967; Johnson and Clayton, 2003; Clayton et al., 2008). The lake continued to evolve and infill, with the northwards-dipping reflectors interpreted as delta foresets (RF3) indicating that lake infill was primarily a result of rapid fan/delta progradation, burying the early phases of esker sedimentation (Fig. 9D). The stacked units (e.g. northern end of line 166) (Fig. 8E) indicate multiple pulses of rapid sediment deposition relating to the continued downwasting of ice, changing stream inputs and expansion of the lake. The final stage of lake infill is represented by the uppermost faint sub-horizontal reflectors (RF4), interpreted as draped lake deposits and topsets (Fig. 9E). These are located towards the central part of the ice-walled lake plain, consistent with the deepest parts of the lake (Clayton and Cherry, 1967; Clayton et al., 2008). The relative lack of fine-grained lake deposits, common in other ice-walled lake plains (e.g. Winters, 1961; Clayton and Cherry, 1967; Johnson and Clayton, 2003; Clayton et al., 2008), suggests that lake progradation and infilling may have been rapid. Subsequent de-icing and removal of ice walls then revealed an upstanding ice-walled lake plain, with sediment collapse likely towards the flanks (e.g. Holmes, 1947; Winters, 1961; Brodzikowski and van Loon, 1991; Huddart, 1981; Clayton et al., 2001, 2008; Johnson and Clayton, 2003; Livingstone et al., 2010a) (Fig. 9F).

The sedimentological and radar data from the esker ridges investigated at the Morley, Brampton and Carlatton Farm sites highlight significant variations in flow conditions. The Morley Farm esker ridge sediment and radar facies indicate low

energy flows, characterised by planar bedded sands and shallow trough features, with little apparent variation in flow conditions evident in the ridge cross-profiles (Fig. 5). By contrast, the Brampton Farm section (Fig. 6A) contains variations in grain sizes (bedded sands to gravel sheets) and evidence of significant deformation. Faulting (e.g. Fig. 6D) is consistent with gravitational deformation indicative of sediment pile let-down or removal of supporting ice walls (e.g. McDonald and Shilts, 1975; Brennand, 2000; Fiore et al., 2002; Livingstone et al., 2010a), and hydrofracturing (e.g. Fig. 6F) indicates fluctuating water pressures (e.g. Lee et al., 2015). The Carlatton Farm GPR long-profile (Fig. 7B) shows evidence of multiple phases of sediment accretion, recording changes in flow conditions both vertically within the ridge and laterally across the long-profile. We suggest the identified variations in flow conditions recorded by the sediment and GPR data are also consistent with differences in overall esker ridge morphologies (e.g. Burke et al. 2015) and their context within the kame belt. Both the Morley and Carlatton Farm sites are within large S-N aligned ridges that form part of a consistent esker ridge network extending northwards through the kame belt (Fig. 2B). We suggest these ridges record stable meltwater drainage routes, characterised by both largely homogenous sedimentation in cross-profile (e.g. Figs. 5 and 7C) and multiple phases of accretion evident along-section. The greater variation in flow conditions recorded in the Carlatton Farm profiles is likely to reflect the complex morphology of the esker ridge (i.e. multiple ridge crests and branches leading off the main ridge; Fig. 7A) compared to Morley Farm (Fig. 5C). The Brampton Farm ridges are smaller and form part of a more-fragmented system aligned broadly SW-NE (Figs. 2B and 3B). Variation in grain size, evidence for fluctuating water pressures (hydrofracture) and hyperconcentrated flows, indicate availability of large sediment volumes and rapid ridge formation (Fiore et al., 2002; Mäkinen, 2003). Evidence for

faulting suggests that the channel system subsequently underwent significant modification during dead ice melt out as supporting ice-walls were removed, consistent with englacial or supraglacial deposition (e.g. Lewis, 1949; Huddart, 1981; Burke et al., 2008) and/or formation in an ice-marginal position (e.g. Storrar et al., in revision).

Evolution of complex kame belts during deglaciation

Two types of drainage network can be identified within the Brampton Kame Belt, providing insight into the formation of kame belts as glacier karst evolves during deglaciation. These are (1) major stable drainage axes that collapsed into a chain of ice-walled lakes as glacier karst develops; and (2) fragmentary ice-marginal esker ridges that formed at or close to the margin between active glacier ice and ice stagnation terrain during recession south-east along the Vale of Eden (Fig. 10).

We suggest that the broadly S-N and SE-NW aligned esker ridges in the south and central parts of the kame belt, trending to SW-NE in the north, record major meltwater drainage axes in this part of the ice sheet (Fig. 10). These esker ridges are consistent with a continuation of the meltwater channel system that extends for tens of kilometres along the western side of the Pennine escarpment (Arthurton & Wadge, 1981; Greenwood et al., 2007; Livingstone et al., 2008, 2010a). The largest esker ridges within the kame belt, including the Brampton ridge (Fig. 2B), follow this general alignment, and therefore their size is likely a function both of the stability of the drainage network and the focusing of sediment and water down these axes. The internal data from the Morley Farm and Carlatton Farm esker ridges (Figs. 5 and 7) show multiple phases of accretion and a lack of pervasive deformation, consistent with a subglacial drainage network. We propose that evolution and continued downwasting

of major subglacial drainage axes during deglaciation led to the formation of a series of aligned ice-walled lakes within a well-developed and stable glacier karst system, as supported by the linear distribution of ice-walled lake plains within the kame belt (e.g. Holmes, 1947) (Figs. 2B and 10A). We suggest this is analogous to the linear chains of supraglacial ponds observed on the debris-covered tongue of Tasman Glacier, New Zealand (Röhl, 2008) (Fig. 11A). The presence of major drainage axes initiated collapse of overlying ice (unroofing), causing a drainage reorganisation and localised ponding of water where channels became blocked by dead ice and debris within the glacier karst. As the ice continued to stagnate and the glacier karst expanded and stabilised, so did the ice-walled lakes (e.g. Holmes, 1947; Lewis, 1949; Clayton, 1964; Evans et al., 2018). The presence of thick (>5 m) sequences of delta foresets dipping northwards within the North Scales ice-walled lake plain (Fig. 8), and the evidence for rapid infilling of lakes (inferred from the relative lack of fine-grained lake deposits identified in the radar data), is consistent with major drainage axes and suggest a large supraglacial debris source, such as the Penrith sandstone ridge and/or the flanks of the Pennine escarpment (Livingstone et al., 2010a).

A series of smaller, more-fragmentary esker ridges aligned SW-NE in the southern part of the kame belt are interpreted to represent deposition in channels running parallel to the south-east retreating ice margin up the Vale of Eden and towards the Stainmore Gap (Fig. 10) (Huddart, 1981; Livingstone et al., 2010a; 2015). A number of these ridges have complex, multi-branched morphologies, including at Brampton Farm (Fig. 6). The sedimentological and radar data from the Brampton Farm esker ridge suggest that formation was likely to have been rapid and associated with fluctuating water pressures and high sediment availability. Evidence for significant deformation is consistent with a partially englacial/supraglacial component to the

drainage channels and the subsequent collapse caused by ice ablation (e.g. Lewis, 1949; Fiore et al., 2002). Eskers formed partly in englacial/supraglacial positions are also consistent with the fragmentary nature of the ridges in this part of the kame belt. Together, these observations suggest late-stage ice-marginal formation during deglaciation, with partial englacial and supraglacial sections to the drainage, contrasting with the relatively stable S-N major drainage axes (Fig. 10). The inferred ice-marginal eskers are consistent with observations of complex polyphase esker systems formed on modern glacier forelands, some of which mimic the shape of the ice margin in addition to the flow-parallel orientation typically associated with eskers (Fig. 11B) (e.g. Storrar et al., in revision). Ice-marginal eskers form where meltwater supply and sedimentation are high, channel abandonment and drainage network reorganisation are frequent and dynamic (e.g. Trotter, 1929; Lewis, 1949; Huddart, 1981), and where the glacier front consists of a defined margin between active glacier ice and ice stagnation terrain (Storrar et al., in revision). We therefore suggest the ice-marginal eskers within the Brampton Kame Belt were formed as water drained from active ice onto the dead ice zone.

GPR as a tool for investigating kame belt stratigraphy and architecture

The GPR profiles provided good insight into the internal structure of landforms within the kame belt, in accordance with previous work in modern and ancient glaciofluvial environments (e.g. Russell et al., 2001; Fiore et al., 2002; Cassidy et al., 2003; Burke et al., 2008, 2015; Winsemann et al., 2018). In particular, the 100 MHz GPR data were effective at capturing broad scale architectural elements, including vertical and lateral variations in styles of sediment accretion (e.g. lateral, headward, downflow or vertical

accretion), and the morphology of boundaries and contacts (e.g. troughs, hummocky surfaces). We also used the GPR data to identify changes in grain size (e.g. bedded sands versus gravel sheets) and depositional structures (e.g. planar, cross-bedded), but in these cases it was important to have sedimentary sections that acted as tie points to identify key radar facies (e.g. Fig. 4). The wider geomorphological and sedimentological context of a site is also important when interpreting radar facies. For instance, at North Scales (Fig. 8), we suggest dipping reflectors are likely to be backsets in some profiles (as opposed to foresets) because the dip direction of the reflectors was opposite to the general S-N/SW-NE trend of meltwater drainage (cf. Fiore et al., 2002; Burke et al., 2008). The GPR data were not effective for identifying individual features, such as hydrofracturing or faulting, even where this was shown to be significant within a sedimentary section (e.g. Fig. 6). The difficulty in picking out finer scale detail may be due to artefacts/noise in the GPR data (e.g. reflectors from trees, fences etc.). The use of a radar system with shielded antenna could be one way to try and improve this in future surveys. Finally, wherever possible, we advocate a combined geomorphological, sedimentological and geophysical approach to the study of complex glaciofluvial sediment-landform assemblages.

Conclusions

Our combined geomorphological, sedimentological and geophysical investigation provides a new assessment of the morphology and internal stratigraphy and architecture of the Brampton Kame Belt. We present a conceptual model for the formation of ice-walled lake plains based on our interpretation of GPR profiles, building on and adding to the body of existing work on this topic. The process-form model suggests that major drainage pathways collapse into a chain of ice-walled lakes as

glacier karst develops during deglaciation. Sediment and GPR data demonstrate significant variation in esker ridge internal structure, indicating differences in flow conditions, styles of accretion, and degree of deformation that can be linked to observed differences in ridge morphologies. The morphology, orientation and internal structure of esker ridges and ice-walled lake plains allow two main styles of drainage to be identified within the kame belt: (1) major drainage axes broadly oriented S-N that collapsed to form a series of aligned ice-walled lakes during the development of relatively stable glacier karst; and (2) ice-marginal drainage systems oriented SW-NE that formed parallel to the margin between active glacier ice and ice stagnation terrain as the ice sheet downwasted and retreated to the south-east during deglaciation. These esker ridges are likely to have formed rapidly and undergone significant modification during dead ice melt out. Our study demonstrates that GPR data provides good insight into the broad scale internal stratigraphy and architecture of landforms in complex kame belts, including variations in accretion styles and boundary morphology. However, sediment exposures are important to help tie sediments to radar facies and to validate interpretations.

References

Allen JRL. 1984. Parallel lamination developed from upper-stage plane beds: a model based on the larger coherent structures of the turbulent boundary layer. Sediment. Geol. 39: 227-242.

Arthurton RS, Wadge AJ. 1981. Geology of the Country around Penrith. Memoir of the British Geological Survey, HMSO, London.

Attig JW, Clayton L. 1993. Stratigraphy and origin of an area of hummocky glacial topography, northern Wisconsin, USA. Quaternary International 18: 61-67. DOI: 10.1016/1040-6182(93)90054-J

Attig JW, Rawling III JE. 2018. Influence of persistent buried ice on late glacial landscape development in part of Wisconsin's Northern Highlands. In Quaternary Glaciation of the Great Lakes Region: Process, Landforms, Sediments, and Chronology, Kehew AE, Curry BB (eds). Geol. Soc. Am. Spec. Paper 530: 103–114.

Auton CA. 1992. Scottish landform examples—6: The Flemington eskers. Scottish Geographical Magazine 108(3): 190-196.

Banerjee I, McDonald BC. 1975. Nature of esker sedimentation. In Glaciofluvial and Glaciolacustrine Sedimentation, Jopling AV, McDonald BC (eds). Soc. Econ. Paleontol. Mineral., Spec. Publ. 23: 304-320.

Bennett GL, Evans DJA. 2012. Glacier retreat and landform production on an overdeepened glacier foreland: the debris-charged glacial landsystem at Kvíárjökull, Iceland. Earth Surface Processes and Landforms 37(15): 1584-1602. DOI:10.1002/esp.3259

Brennand TA. 1994. Macroforms, large bedforms and rhythmic sedimentary sequences in subglacial eskers, south-central Ontario: implications for esker genesis and meltwater regime. Sedimentary Geology 91(1-4): 9-55.

Brennand TA. 2000. Deglacial meltwater drainage and glaciodynamics: inferences from Laurentide eskers, Canada. Geomorphology 32(3-4): 263-293. DOI: 10.1016/S0169-555X(99)00100-2

Brodzikowski K, van Loon AJ. 1991. Glacigenic sediments. Elsevier: Oxford.

Burke MJ, Woodward J, Russell AJ, Fleisher PJ, Bailey PK. 2008. Controls on the sedimentary architecture of a single event englacial esker: Skeiðarárjökull, Iceland. Quaternary Science Reviews 27(19-20): 1829-1847. DOI: 10.1016/j.quascirev.2008.06.012

Burke MJ, Brennand TA, Sjogren DB. 2015. The role of sediment supply in esker formation and ice tunnel evolution. Quaternary Science Reviews 115: 50-77. DOI: 10.1016/j.quascirev.2015.02.017

Busby JP, Merritt JW. 1999. Quaternary deformation mapping with ground penetrating radar. Journal of Applied Geophysics 41(1): 75-91. DOI: 10.1016/S0926-9851(98)00050-0

Cassidy NJ, Russell AJ, Marren PM, Fay H, Knudsen O, Rushmer EL, Van Dijk TAGP. 2003. GPR derived architecture of November 1996 jökulhlaup deposits, Skeiðarársandur, Iceland. Geological Society, London, Special Publications 211(1): 153-166. DOI: 10.1144/GSL.SP.2001.211.01.13

Chandler BM, Lovell H, Boston CM, Lukas S, Barr ID, Benediktsson ÍÖ, Benn DI, Clark CD, Darvill CM, Evans DJA, Ewertowski MW, Loibl D, Margold M, Otto J-C, Roberts DH, Stokes CR, Storrar RD, Stroeven AP. 2018. Glacial geomorphological mapping: A review of approaches and frameworks for best practice. Earth-Science Reviews 185: 806-846. DOI: 10.1016/j.earscirev.2018.07.015

Clark CD, Hughes AL, Greenwood SL, Jordan C, Sejrup HP. 2012. Pattern and timing of retreat of the last British-Irish Ice Sheet. Quaternary Science Reviews 44: 112-146. DOI: 10.1016/j.quascirev.2010.07.019

Clark CD, Ely JC, Greenwood SL, Hughes AL, Meehan R, Barr ID, Bateman MD, Bradwell T, Doole J, Evans DJA, Jordan CJ, Monteys X, Pellicer XM, Sheehy M. 2018. BRITICE Glacial Map, version 2: a map and GIS database of glacial landforms of the last British–Irish Ice Sheet. Boreas 47(1): 11-27. DOI: 10.1111/bor.12273

Clayton L. 1964. Karst topography on stagnant glaciers. Journal of Glaciology 5(37): 107-112. DOI: 10.3189/S0022143000028628

Clayton L. 1967. Stagnant-glacier features of the Missouri Coteau in North Dakota. North Dakota Geological Survey, Miscellaneous Series 30: 25-46.

Clayton L, Cherry JA. 1967. Pleistocene superglacial and ice-walled lakes of west-central North America. North Dakota Geological Survey, Miscellaneous Series 30: 47-52.

Clayton L, Attig JW, Mickelson DM. 2001. Effects of late Pleistocene permafrost on the landscape of Wisconsin, USA. Boreas 30(3): 173-188. DOI: 10.1111/j.1502-3885.2001.tb01221.x

Clayton L, Attig JW, Ham NR, Johnson MD, Jennings CE, Syverson KM. 2008. Ice-walled-lake plains: Implications for the origin of hummocky glacial topography in middle North America. Geomorphology 97(1-2): 237-248. DOI: 10.1016/j.geomorph.2007.02.045

Cook JH. 1946. Kame complexes and perforation deposits. American Journal of Science 244(8): 573-583. DOI: 10.2475/ajs.244.8.573

Curry B, Petras J. 2011. Chronological framework for the deglaciation of the Lake Michigan lobe of the Laurentide Ice Sheet from ice-walled lake deposits. Journal of Quaternary Science 26(4): 402-410. DOI: 10.1002/jqs.1466

Curtis GC, Woodworth JB. 1899. Nantucket, a morainal island. The Journal of Geology 7(3): 226-236.

Evans DJA, Benn DI (eds.). 2004. A practical guide to the study of glacial sediments. Hodder Education: London.

Evans DJA, Hughes AL, Hansom JD, Roberts DH. 2017. Scottish landform examples 43: Glacifluvial landforms of Strathallan, Perthshire. Scottish Geographical Journal 133(1): 42-53. DOI: 10.1080/14702541.2016.1254276

Evans DJA, Roberts DH, Bateman MD, Ely J, Medialdea A, Burke MJ, Chiverell RC, Clark CD, Fabel D. 2018. A chronology for North Sea Lobe advance and recession on the Lincolnshire and Norfolk coasts during MIS 2 and 6. Proceedings of the Geologists' Association. DOI: 10.1016/j.pgeola.2018.10.004

Fiore J, Pugin A, Beres M. 2002. Sedimentological and GPR studies of subglacial deposits in the Joux Valley (Vaud, Switzerland): backset accretion in an esker followed by an erosive jökulhlaup. Géographie physique et Quaternaire 56(1): 19-32. DOI:10.7202/008602ar

Flint RF. 1928a. Pleistocene terraces of the lower Connecticut Valley. Bulletin of the Geological Society of America 39(4): 955-984. DOI: 10.1130/GSAB-39-955

Flint RF. 1928b. Eskers and crevasse fillings. American Journal of Science: (89), 410-416. DOI: 10.2475/ajs.s5-15.89.410

Flint RF. 1929. The stagnation and dissipation of the last ice sheet. Geographical Review 19(2): 256-289. DOI: 10.2307/208535

Flint RF. 1930. The Origin of the Irish" Eskers". Geographical Review 20(4): 615-630. DOI: 10.2307/209015

Gerke HH, Koszinski S, Kalettka T, Sommer M. 2010. Structures and hydrologic function of soil landscapes with kettle holes using an integrated hydropedological approach. Journal of Hydrology 393(1-2): 123-132. 10.1016/j.jhydrol.2009.12.047.

Gorrell G, Shaw J. 1991. Deposition in an esker, bead and fan complex, Lanark, Ontario, Canada. Sedimentary Geology 72(3-4): 285-314. DOI: 10.1016/0037-0738(91)90016-7

Greenwood SL, Clark CD, Hughes AL. 2007. Formalising an inversion methodology for reconstructing ice-sheet retreat patterns from meltwater channels: application to the British Ice Sheet. Journal of Quaternary Science 22(6): 637-645. DOI: 10.1002/jqs.1083

Heinz J, Aigner T. 2003. Hierarchical dynamic stratigraphy in various Quaternary gravel deposits, Rhine glacier area (SW Germany): implications for hydrostratigraphy. International Journal of Earth Sciences 92(6): 923-938.

Holmes CD. 1947. Kames. American journal of Science 245(4): 240-249. DOI: 10.2475/ajs.245.4.240

Huddart D. 1981. Fluvioglacial systems in Edenside (middle Eden Valley and Brampton kame belt). Field Guide to Eastern Cumbria. Quaternary Research Association: London: 79-103.

Johnson MD, Clayton L. 2003. Supraglacial landsystems in lowland terrain. glacial landsystems. In Glacial Landsystems. Evans DJA (ed). Arnold: London: 228-258.

Jopling AV. Walker RG. 1968. Morphology and origin of ripple-drift cross-lamination, with examples from the Pleistocene of Massachusetts. Journal of Sedimentary Research 38(4): 971-984. DOI: 10.1306/74D71ADC-2B21-11D7-8648000102C1865D

Kayler ZE, Badrian M, Frackowski A, Rieckh H, Nitzsche KN, Kalettka T, Merz C, Gessler A. 2018. Ephemeral kettle hole water and sediment temporal and spatial dynamics within an agricultural catchment. Ecohydrology 11(2): e1929. DOI: 10.1002/eco.1929.

Lee JR, Wakefield OJ, Phillips E, Hughes L. 2015. Sedimentary and structural evolution of a relict subglacial to subaerial drainage system and its hydrogeological implications: an example from Anglesey, north Wales, UK. Quaternary Science Reviews 109: 88-110. DOI: 10.1016/j.quascirev.2014.09.010

Levy A, Robinson Z, Krause S, Waller R, Weatherill J. 2015. Long-term variability of proglacial groundwater-fed hydrological systems in an area of glacier retreat, Skeiðarársandur, Iceland. Earth Surface Processes and Landforms 40(7): 981-994. DOI: 10.1002/esp.3696.

Lewis WV. 1949. An esker in process of formation: Böverbreen, Jotunheimen, 1947. Journal of Glaciology 1(6): 314-319. DOI: 10.3189/S0022143000010066

Lischeid G, Balla D, Dannowski R, Dietrich O, Kalettka T, Merz C, Schindler U, Steidl J. 2017. Forensic hydrology: what function tells about structure in complex settings. Environmental Earth Sciences 76(1): 40. DOI: 10.1007/s12665-016-6351-5.

Livingstone SJ, Ó Cofaigh C, Evans DJA. 2008. Glacial geomorphology of the central sector of the last British-Irish Ice Sheet. Journal of Maps 4(1): 358-377. DOI: 10.4113/jom.2008.1032

Livingstone SJ, Evans DJA, Ó Cofaigh C, Hopkins J. 2010a. The Brampton kame belt and Pennine escarpment meltwater channel system (Cumbria, UK): morphology, sedimentology and formation. Proceedings of the Geologists' Association 121(4): 423-443. DOI: 10.1016/j.pgeola.2009.10.005

Livingstone SJ, Ó Cofaigh C, Evans DJA. 2010b. A major ice drainage pathway of the last British–Irish Ice Sheet: the Tyne Gap, northern England. Journal of Quaternary Science 25(3): 354-370. DOI: 10.1002/jqs.1341

Livingstone SJ., Evans DJA, Ó Cofaigh C (eds). (2010c). The Quaternary of the Solway Lowlands and Pennine escarpment. Quaternary Research Association: London

Livingstone SJ, Roberts DH, Davies BJ, Evans DJA, Ó Cofaigh C, Gheorghiu DM. 2015. Late Devensian deglaciation of the Tyne Gap Palaeo-Ice Stream, northern England. Journal of Quaternary Science 30(8): 790-804. DOI: 10.1002/jqs.2813

Lukas S, Sass O. 2011. The formation of Alpine lateral moraines inferred from sedimentology and radar reflection patterns: a case study from Gornergletscher, Switzerland. Geological Society, London, Special Publications 354(1): 77-92. DOI: 10.1144/SP354.5

Lundqvist J. 1979. Morphogenic classification of glaciofluvial deposits. Sver. Geol. Unders., Ser. C 767: 72.

Maizels JK. 1977. Experiments on the origin of kettle-holes. Journal of Glaciology 18(79): 291-303. DOI: 10.3189/S0022143000021365

Mäkinen J. 2003. Time-transgressive deposits of repeated depositional sequences within interlobate glaciofluvial (esker) sediments in Köyliö, SW Finland. Sedimentology 50(2): 327-360.

Malmberg Persson K. 1991. Internal structures and depositional environment of a kame deposit at V. Ingelstad, Skåne, southern Sweden. GFF 113(2-3): 163-170. DOI: 10.1080/11035899109453850

Mannerfelt CM. 1945. Några glacialmorfologiska Formelement. Geografiska Annaler, 27: 1–239. DOI: 10.1080/20014422.1945.11880740

McDonald B, Shilts WW. 1975. Interpretation of faults in glaciofluvial sediments. In Glaciofluvial and Glaciolacustrine Sedimentation. Jopling AV, McDonald BC. (eds). Soc. Econ. Paleontol. Mineral., Spec. Publ. 23: 123-131.

Miall AD. 1977. A review of the braided-river depositional environment. Earth-Science Reviews 13(1): 1-62. DOI: 10.1016/0012-8252(77)90055-1

Miall AD. 1985. Architectural-element analysis: a new method of facies analysis applied to fluvial deposits. Earth-Science Reviews 22(4): 261-308. DOI: 10.1016/0012-8252(85)90001-7

Paterson J, Cheel RJ. 1997. The depositional history of the Bloomington complex, an ice-contact deposit in the Oak Ridges Moraine, southern Ontario, Canada. Quaternary Science Reviews 16(7): 705-719. DOI: 10.1016/S0277-3791(97)00017-6

Pellicer XM, Gibson P. 2011. Electrical resistivity and Ground Penetrating Radar for the characterisation of the internal architecture of Quaternary sediments in the Midlands of Ireland. Journal of Applied Geophysics: 75(4): 638-647. DOI: 10.1016/j.jappgeo.2011.09.019

Phillips E, Hughes L. 2014. Hydrofracturing in response to the development of an overpressurised subglacial meltwater system during drumlin formation: an example from Anglesey, NW Wales. Proceedings of the Geologists' Association 125(3): 296-311. DOI: 10.1016/j.pgeola.2014.03.004

Price RJ. 1969. Moraines, sandar, kames and eskers near Breidamerkurjökull, Iceland. Transactions of the Institute of British Geographers 46: 17-43. DOI: 10.2307/621406

Rieck RL. 1979. Ice stagnation and paleodrainage in and near an interlobate area. Papers of the Michigan Academy of Sciences, Arts, and Letters 11:219-235.

Rijsdijk KF, Owen G, Warren WP, McCarroll D, van der Meer JJM. 1999. Clastic dykes in over-consolidated tills: evidence for subglacial hydrofracturing at Killiney Bay, eastern Ireland. Sedimentary Geology, 129(1-2): 111-126. DOI: 10.1016/S0037-0738(99)00093-7

Ringrose S. 1982. Depositional processes in the development of eskers in Manitoba. In Research in Glacial, Glacio-Fluvial and Glacio-Lacustrine Systems. Proceedings of the 6th Guelph Symposium on Geomorphology 1980: 117-137.

Röhl K. 2008. Characteristics and evolution of supraglacial ponds on debris-covered Tasman Glacier, New Zealand. Journal of Glaciology 54(188): 867-880. DOI: 10.3189/002214308787779861

Russell AJ, Knudsen O, Fay H, Marren PM, Heinz J, Tronicke J. 2001. Morphology and sedimentology of a giant supraglacial, ice-walled, jökulhlaup channel, Skeiðarárjökull, Iceland: implications for esker genesis. Global and Planetary Change 28(1-4): 193-216. DOI: 10.1016/S0921-8181(00)00073-4

Rust BR, Romanelli R. 1975. Late Quaternary subaqueous outwash deposits near Ottawa, Canada. In Glaciofluvial and Glaciolacustrine Sedimentation. Jopling AV, McDonald BC (eds). Soc. Econ. Paleontol. Mineral., Spec. Publ. 23: 177-192.

Sadura S, Martini IP, Endres AL, Wolf K. 2006. Morphology and GPR stratigraphy of a frontal part of an end moraine of the Laurentide Ice Sheet: Paris Moraine near Guelph, ON, Canada. Geomorphology 75(1-2): 212-225. DOI: 10.1016/j.geomorph.2005.01.014

Saunderson HC. 1977. The sliding bed facies in esker sands and gravels: a criterion for full-pipe (tunnel) flow? Sedimentology 24(5): 623-638. DOI: 10.1111/j.1365-3091.1977.tb00261.x

Schaetzl RJ, Enander H, Luehmann MD, Lusch DP, Fish C, Bigsby M, Steigmeyer M, Guasco J, Forgacs C, Pollyea A. 2013. Mapping the physiography of Michigan using GIS. Physical Geography 34:1-38. DOI: 10.1080/02723646.2013.778531

Schaetzl RJ, Lepper K, Thomas SE, Grove L, Treiber E, Farmer A, Fillmore A, Lee J, Dickerson B, Alme K. 2017. Kame deltas provide evidence for a new glacial lake and suggest early glacial retreat from central Lower Michigan, USA. Geomorphology 280: 167-178. DOI: 10.1016/j.geomorph.2016.11.013

Shulmeister J. 1989. Flood deposits in the Tweed esker (southern Ontario, Canada). Sedimentary Geology 65(1-2): 153-163. DOI: 10.1016/0037-0738(89)90012-2

Spagnolo M, King EC, Ashmore DW, Rea BR. Ely JC, Clark CD. 2014. Looking through drumlins: testing the application of ground-penetrating radar. Journal of Glaciology 60(224): 1126-1134. DOI: 10.3189/2014JoG14J110

Stanley KE, Schaetzl RJ. 2011. Characteristics and paleoenvironmental significance of a thin, dual-sourced loess sheet, north-central Wisconsin. Aeolian Research 2(4): 241-251. DOI: 10.1016/j.aeolia.2011.01.001

Storrar R, Ewertowski M, Tomczyk AM, Barr ID, Livingstone SJ, Ruffell A, Stoker BJ, Evans DJA. In revision. Equifinality and preservation potential of complex eskers. Boreas. Pre-print available at: https://eartharxiv.org/me879/

Thomas GSP, Montague E. 1997. The morphology, stratigraphy and sedimentology of the Carstairs Esker, Scotland, UK. Quaternary Science Reviews 16(7): 661-674. DOI: 10.1016/S0277-3791(97)00014-0

Trotter FM. 1929. The glaciation of eastern Edenside, the Alston block, and the Carlisle plain. Quarterly Journal of the Geological Society 85(1-4): 549-612. DOI: 10.1144/GSL.JGS.1929.085.01-04.17

van der Meer JJM, Kjær KH, Krüger J, Rabassa J, Kilfeather AA. 2009. Under pressure: clastic dykes in glacial settings. Quaternary Science Reviews 28(7-8): 708-720. DOI: 10.1016/j.quascirev.2008.07.017

Warren WP, Ashley GM. 1994. Origins of the ice-contact stratified ridges (eskers) of Ireland. Journal of Sedimentary Research 64(3a): 433-449. DOI: 10.1306/D4267DD9-2B26-11D7-8648000102C1865D

Winsemann J, Lang J, Polom U, Loewer M, Ige J, Pollok L, Brandes C. 2018. Ice-marginal forced regressive deltas in glacial lake basins: geomorphology, facies

variability and large-scale depositional architecture. Boreas 47(4): 973-1002. DOI: https://doi.org/10.1111/bor.12317

Woodward J, Burke MJ. 2007. Applications of ground-penetrating radar to glacial and frozen materials. Journal of Environmental and Engineering Geophysics 12(1): 69-85.

Woodworth JB. 1894. Some typical eskers of southern New England. Proceedings of the Boston Society of Natural History 26: 197-220.

Acknowledgements
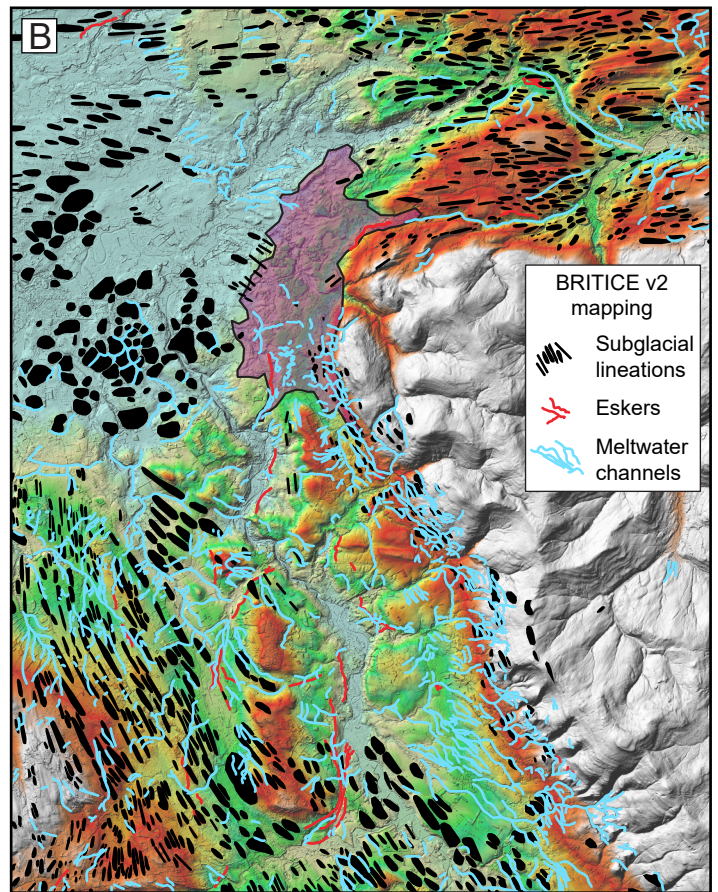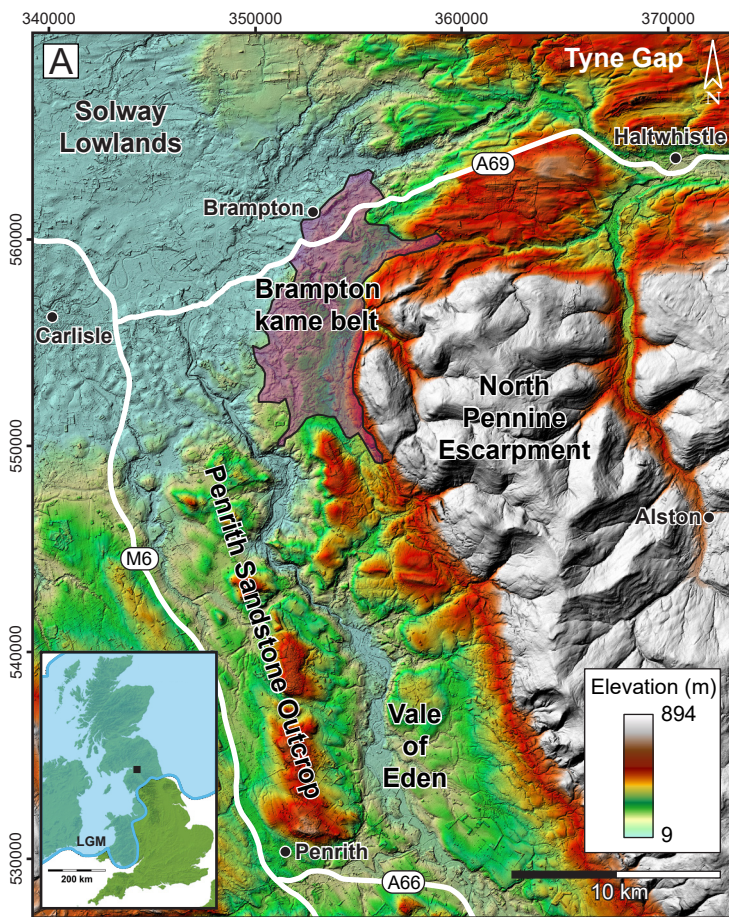
Figure 1 – Location map of the Brampton Kame Belt. Underlying image is shaded relief NEXTMap data. (A) Kame belt location relative to the topography of the area and major towns and roads. Inset shows location of the study area in the central sector of the British-Irish Ice Sheet. Last Glacial Maximum (LGM) limit is 'Scenario One – 27ka' in Clark et al. (2012). (B) The kame belt in the context of the regional glacial geomorphology. Mapping is from the BRITICE Glacial Map version 2 (Clark et al., 2018).
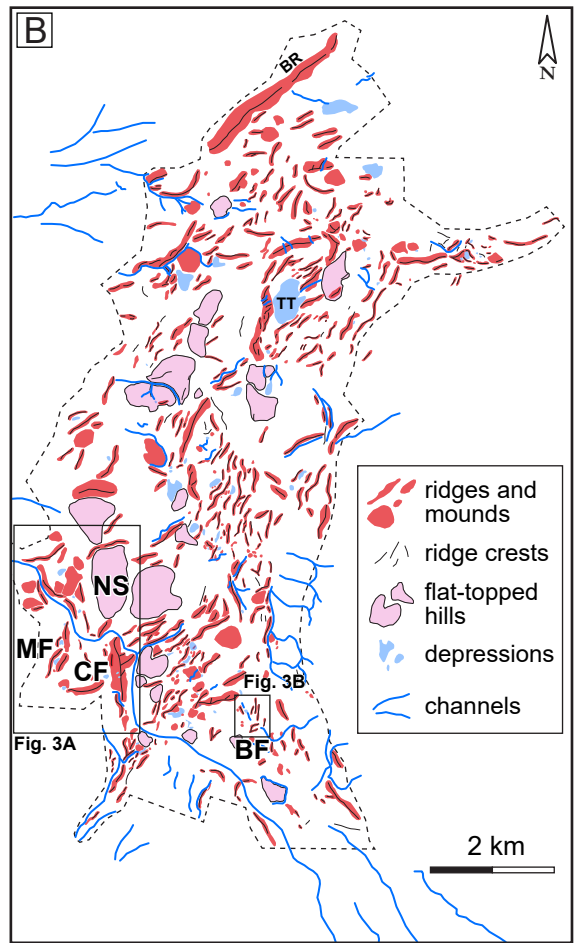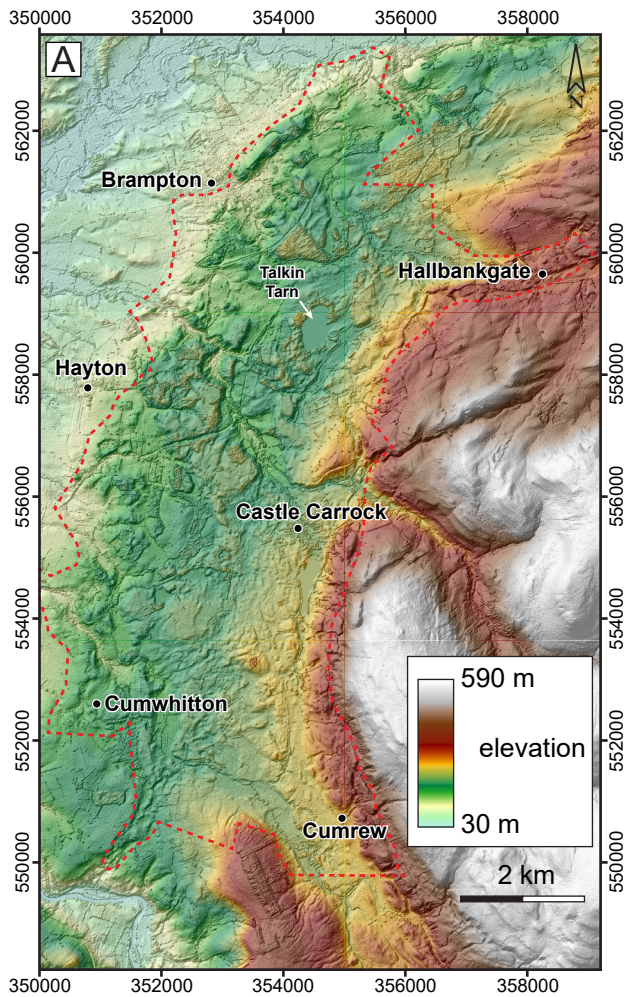
Figure 2 – (A) NEXTMap mosaic showing the topography of the Brampton Kame Belt (dashed red line delimits kame belt boundary). (B) Geomorphological map of the Brampton Kame Belt (dashed black line delimits kame belt boundary). Sites of GPR lines and sediment sections presented in the paper: MF = Morley Farm, BF = Brampton Farm, CF = Carlatton Farm, NS = North Scales. Additional locations of relevance: BR = Brampton ridge, TT = Talkin Tarn.
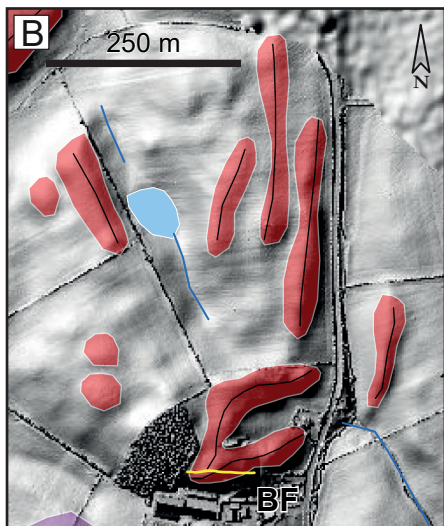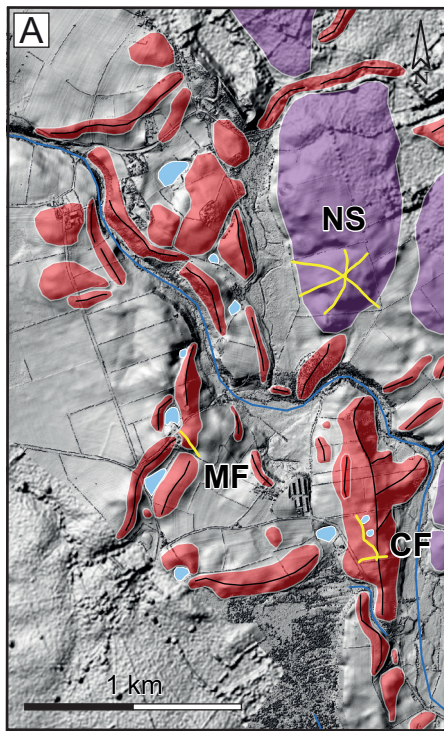
Figure 3 – Location and geomorphological context of GPR lines (in yellow) presented in this study. Underlying images are 1 m resolution DSMs. Mapped landforms are esker ridges (in red), ice-walled lake plains (in purple), kettles (in light blue), and meltwater channels (blue lines). (A) Morley Farm (MF), Carlatton Farm (CF) and North Scales (NS) sites. (B) Brampton Farm (BF) site.
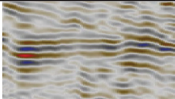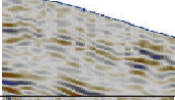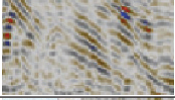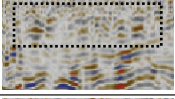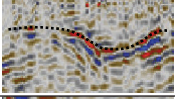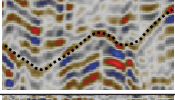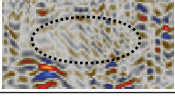
Radar facies	Example	Characteristics	Interpretation
RF1		Continuous and strong sub-horizontal to wavy reflectors	Sub-horizontally bedded sands
RF2		Discontinuous sub-horizontal reflectors	Gravel sheets/layers. In some cases may represent deformed sediment packages
RF3		Dipping relfectors, sometimes discontinuous and often downlapping onto underlying radar surfaces	Foresets/backsets
RF4		Faint sub-horizontal reflectors, typically overlying RF3 and in places mimicking underlying radar surfaces	Topsets/draped lake sediments
RF5		Continuous and discontinuous undulating reflectors with a hummocky upper surface mimicking underlying reflectors	Ridge-scale sedimentation (macroforms) within an ice-walled channel. In some contexts could be subaqueous fan deposits
RF6		Trough-shaped features containing sub-horizontal reflectors	Channels, either continuous sedimentation within migrating system, or incised and infilled
RF7		Disorganised reflectors, steeply-angled in places. Can include offset reflectors, possible evidence for faulting	Deformed sediment packages

Figure 4 – Radar facies classification used to describe and interpret the GPR profiles.
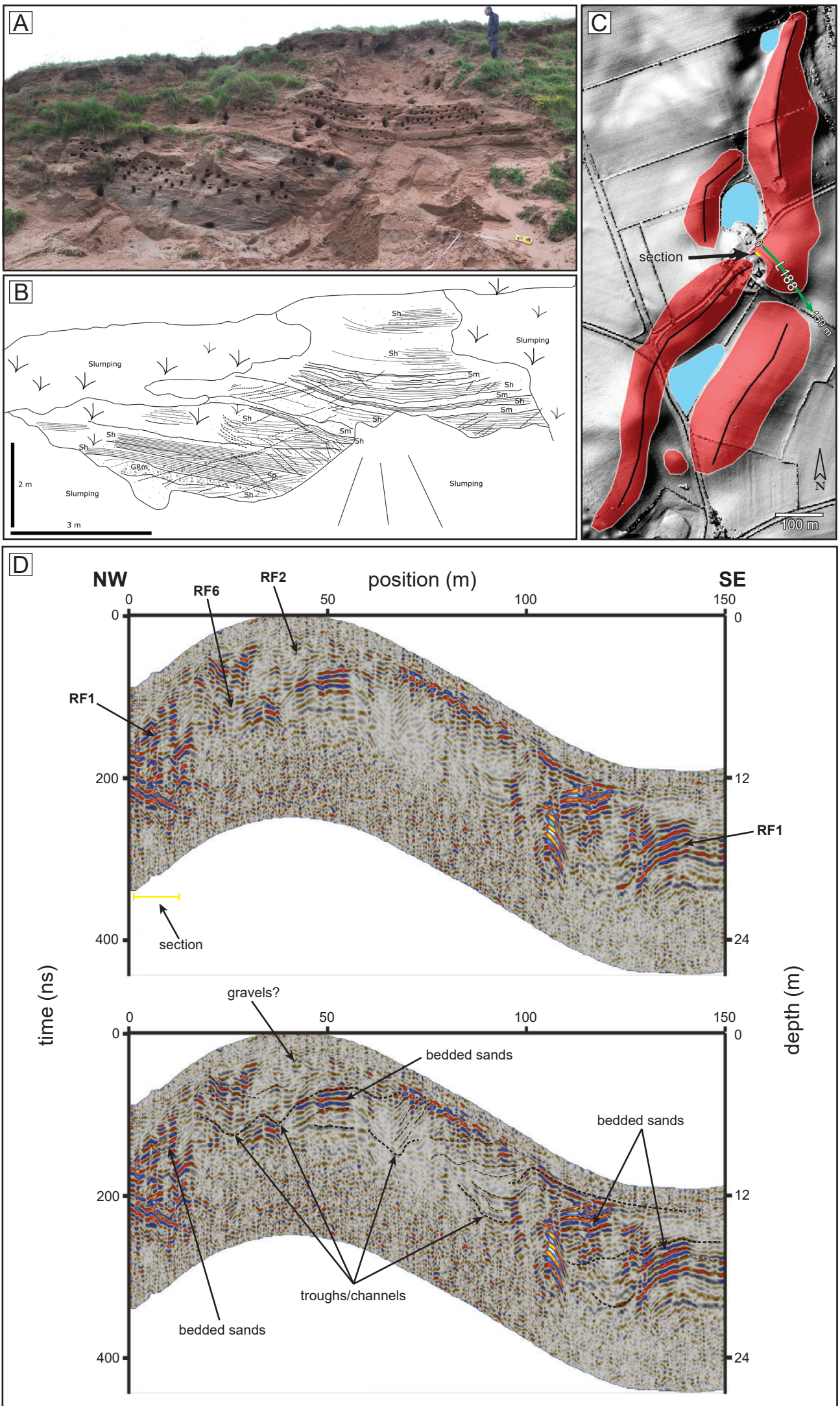
Figure 5 – Morley Farm site. (A) Section photo. (B) Sediment log. (C) DSM showing mapped esker ridges (in red) and kettles (in light blue) with location of section (yellow line) and GPR line 188 (green arrow). (D) GPR line 188 and annotated interpretation of GPR data. See text and Fig. 4 for reference to numbered radar facies (RF). Approximate location of section in (A) and (B) is indicated by the yellow line in the top panel. See Figs. 2B and 3A for location of site.
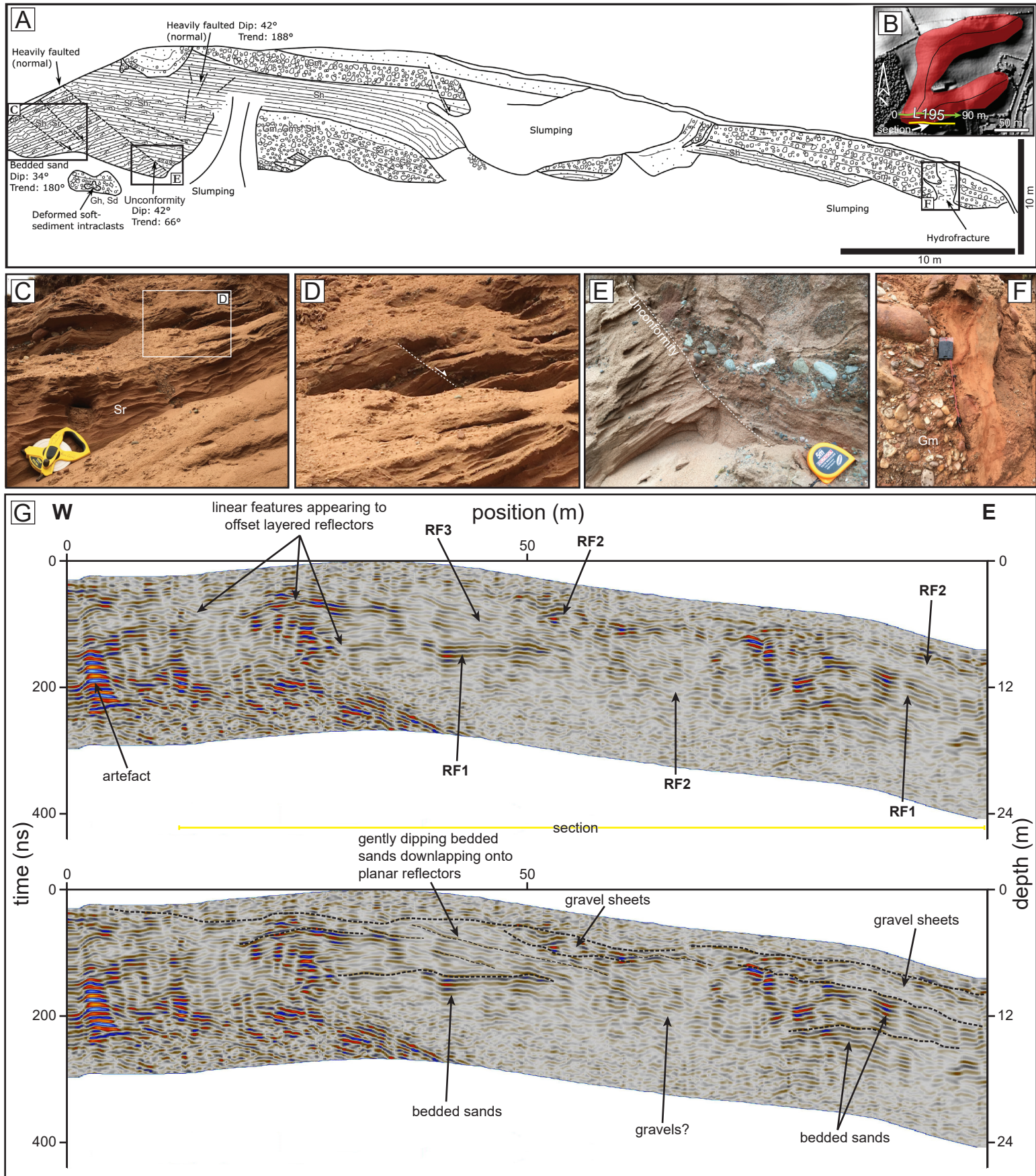
Figure 6 – Brampton Farm site. (A) Sediment log. (B) DSM showing mapped esker ridges (in red) and location of section (yellow line) and GPR line 195 (green arrow). (C) to (F) Photographs showing close-up of details in (A). (G) GPR line 195 and annotated interpretation of GPR data. See text and Fig. 4 for reference to numbered radar facies (RF). Approximate location of section in (A) is indicated by the yellow line in the top panel. The diagonal swipes to the west end of the section are thought to be artefacts from trees located at the edge of the field. See Figs. 2B and 3B for location of site.
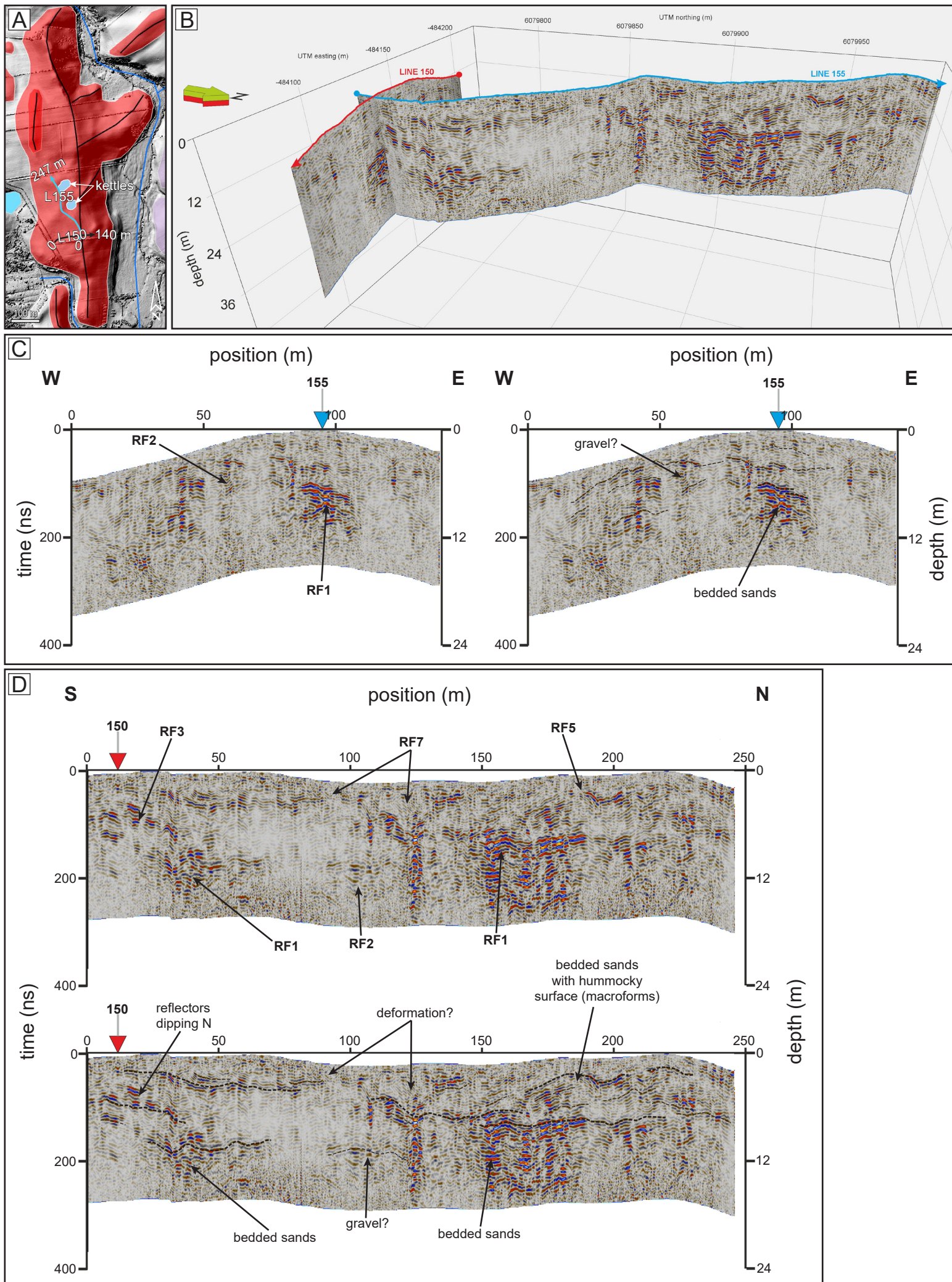
Figure 7 – GPR lines 150 and 155 collected from the Carlatton Farm esker ridge. (A) DSM showing mapped esker ridges (in red), ice-walled lake plains (in purple), kettles (in light blue), and meltwater channels (blue lines) with location of GPR lines 150 (black arrow) and 155 (blue arrow). See Figs. 2B and 3A for location of site. (B) Fence diagram of lines. (C) Line 150 and annotated interpretations. (D) Line 155 and annotated interpretations. See text and Fig. 4 for reference to numbered radar facies (RF) in (C) and (D).
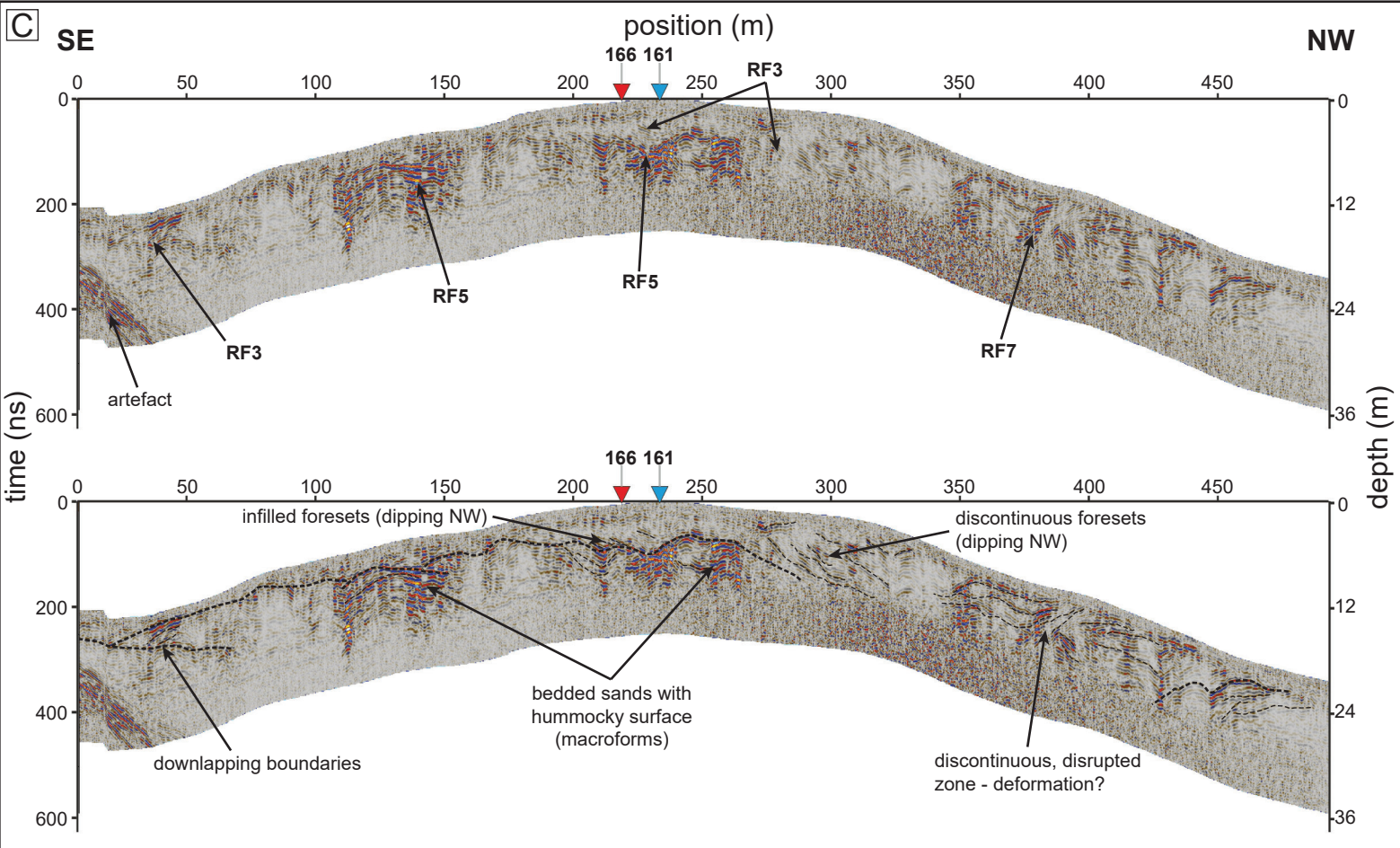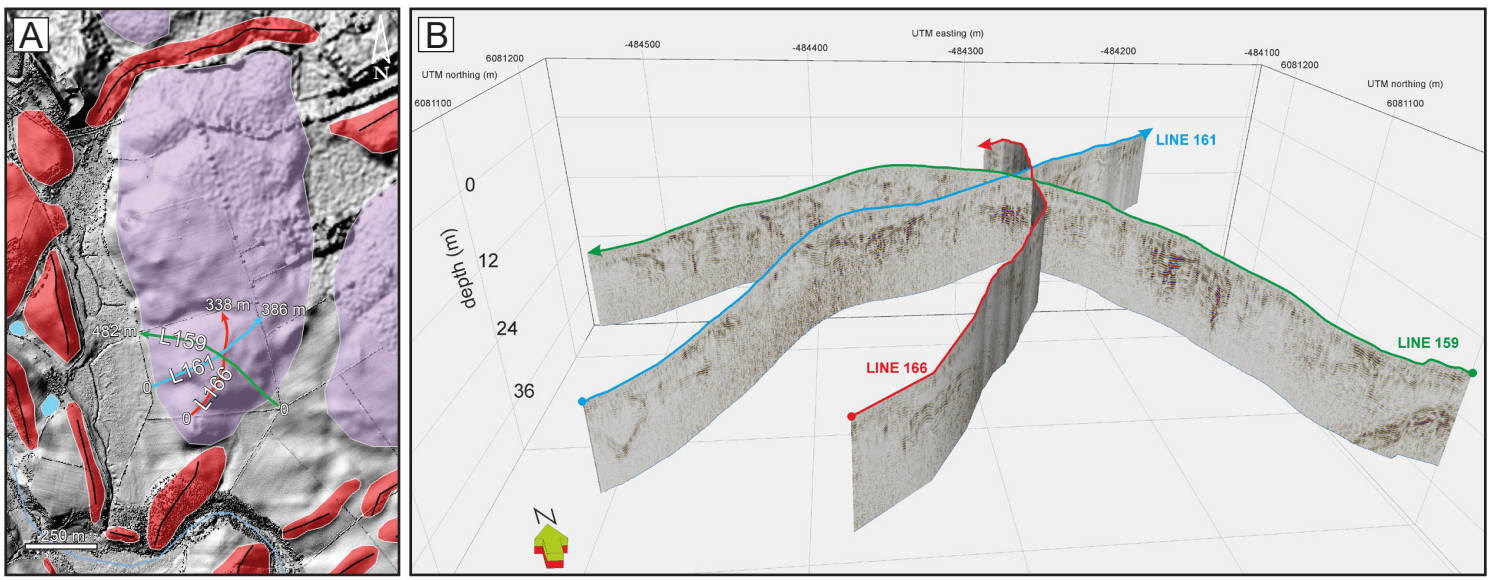
Figure 8 – GPR lines 159, 161 and 166 collected from North Scales ice-walled lake plain. (A) DSM showing mapped ice-walled lake plain (in purple), esker ridges (in red), kettles (in light blue), and meltwater channels (blue lines) with location of GPR lines 159 (green arrow), 161 (blue arrow) and 166 (red arrow). See Figs. 2B and 3A for location of site. (B) Fence diagram of lines. (C) Line 159 and annotated interpretations. (D) Line 161 and annotated interpretations. (E) Line 166 and annotated interpretations. See text and Fig. 4 for reference to numbered radar facies (RF) in (C), (D) and (E).
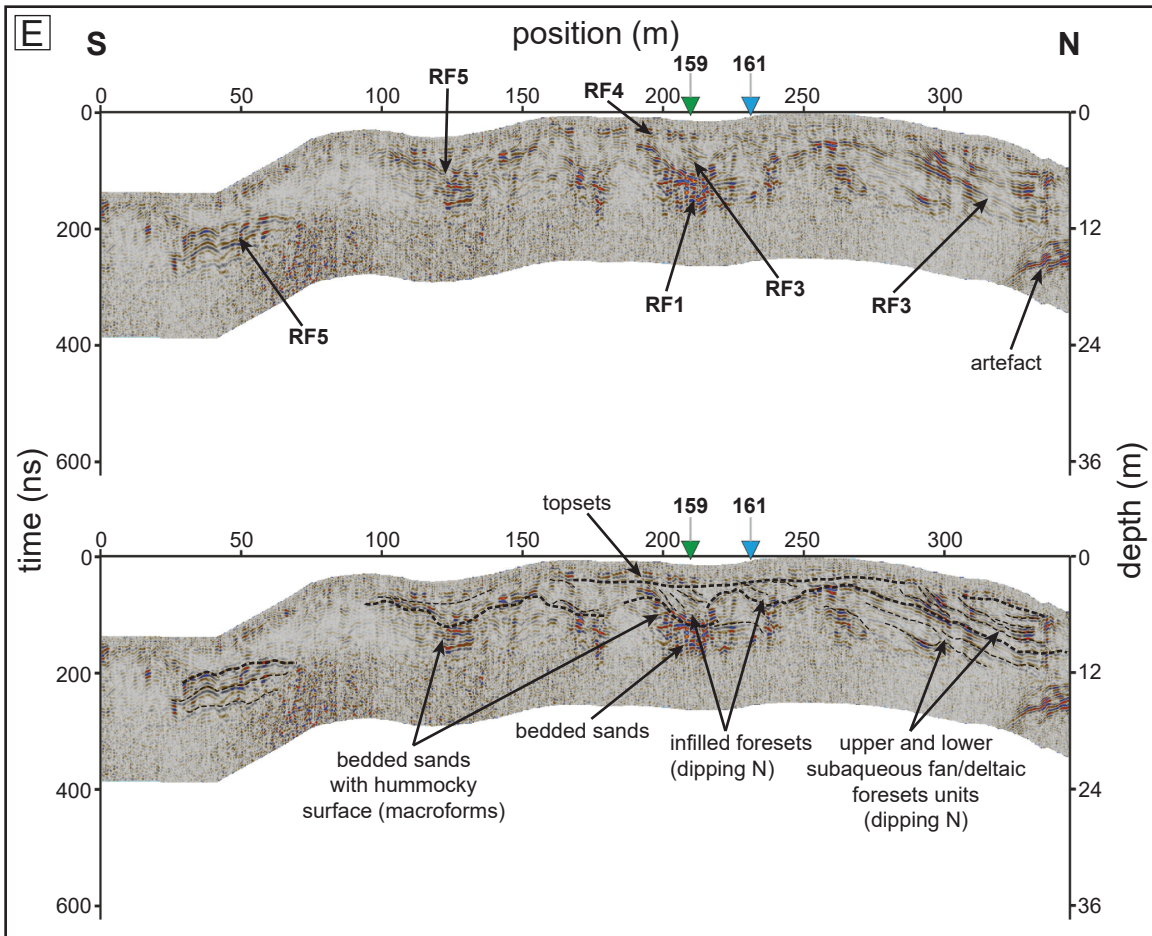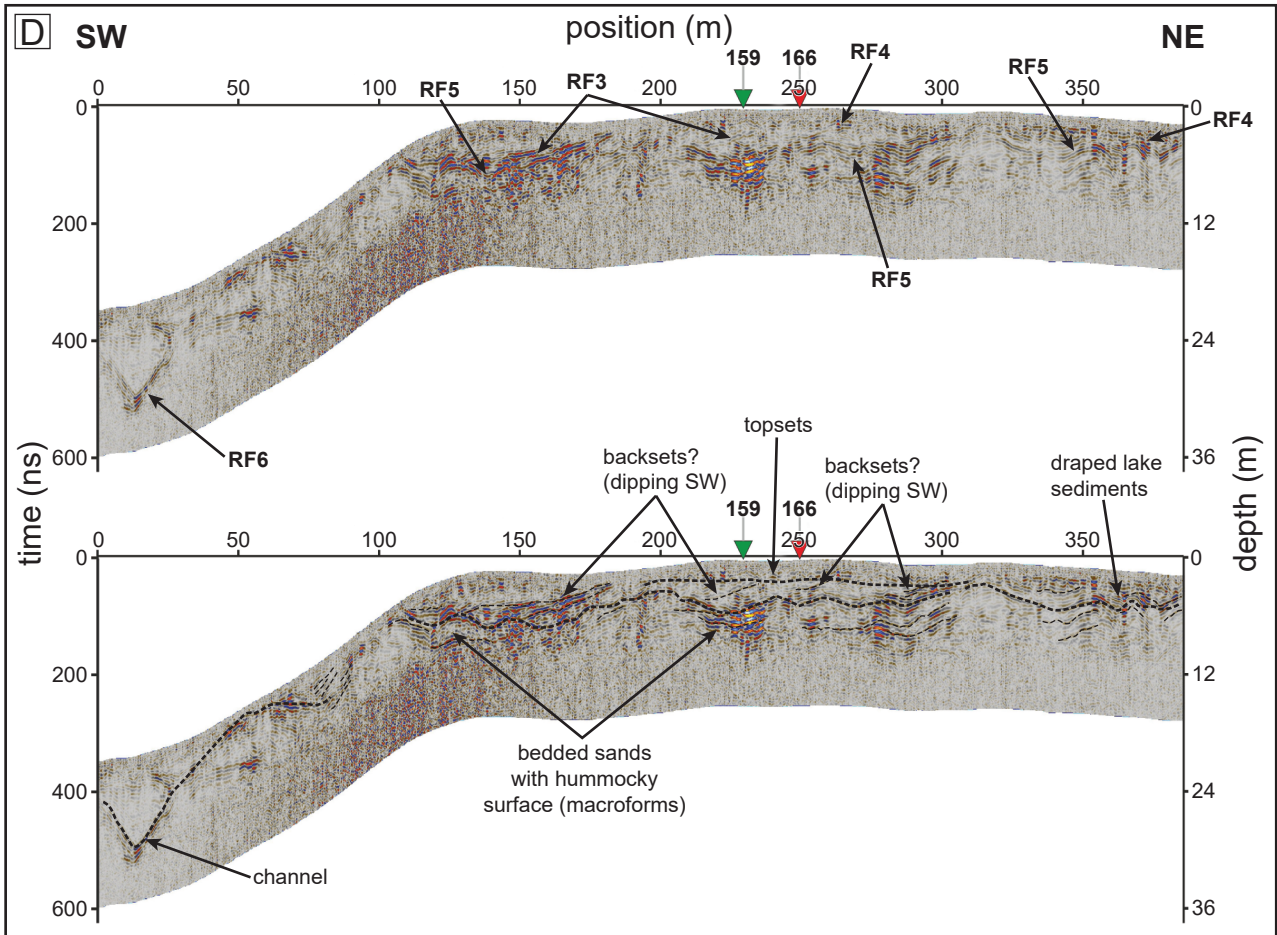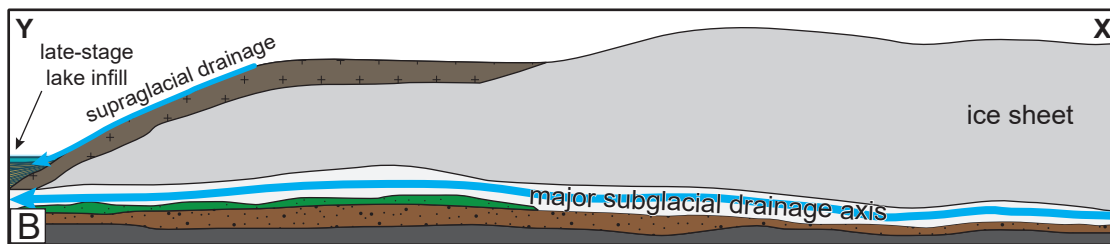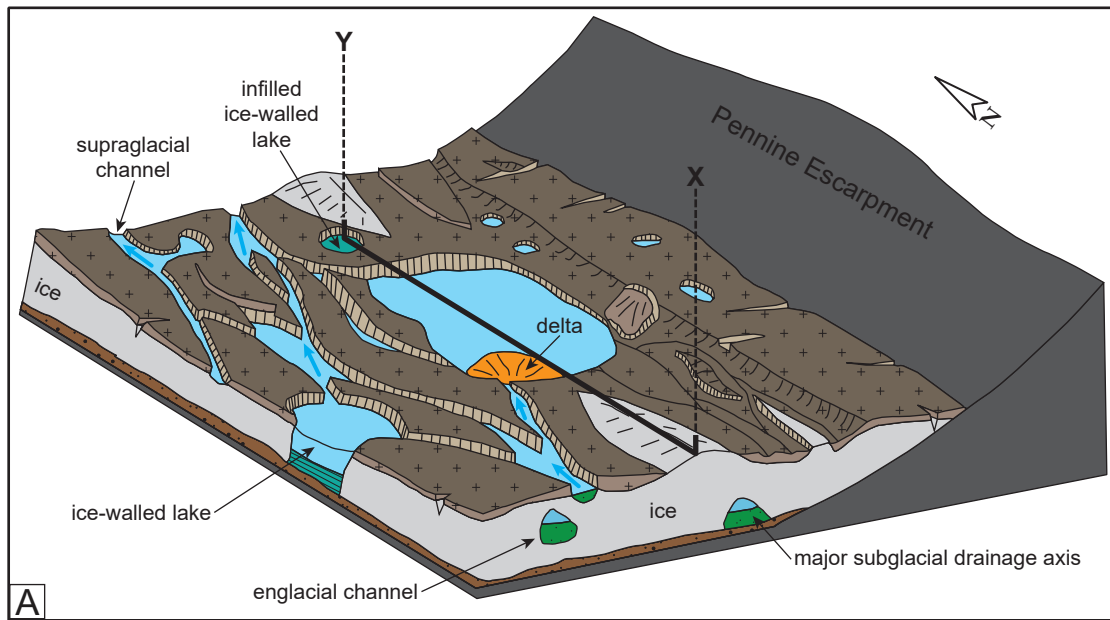
Figure 8 – continued
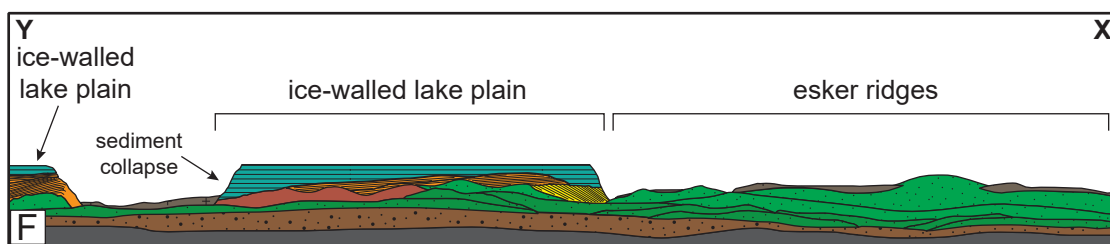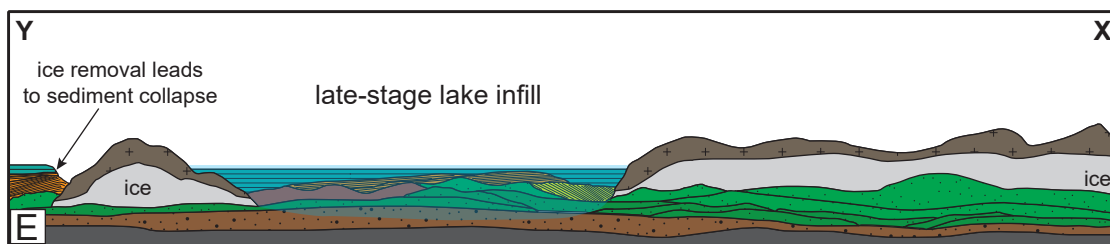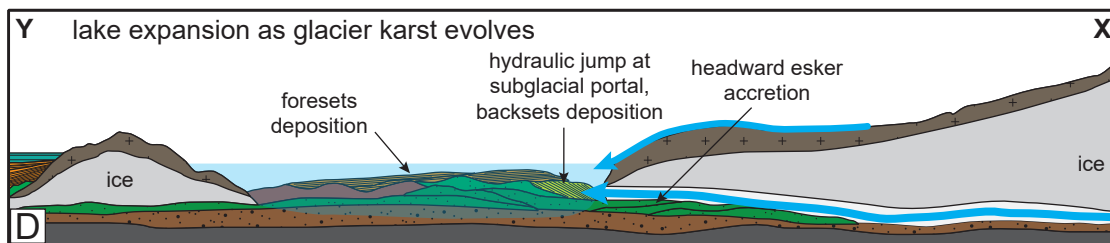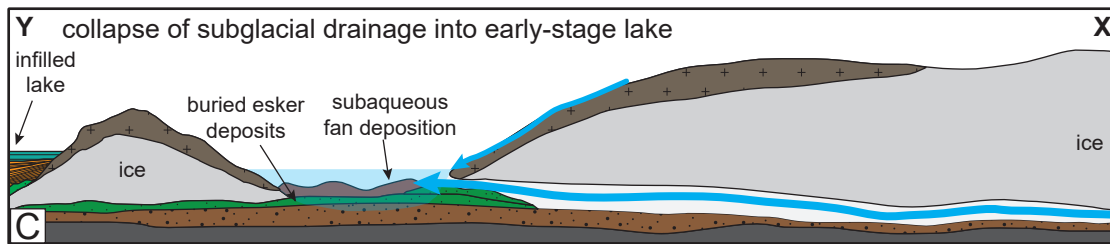
Figure 9 – Conceptual model showing formation of North Scales ice-walled lake plain and esker ridges based on interpretation of GPR data. (A) Brampton Kame Belt conceptual model, adapted from Livingstone et al. (2010c). Panels (B) to (F) are two-dimensional cross-sections showing the evolution of a section of the kame belt along the transect X-Y, which transitions from a major subglacial drainage channel into an ice-walled lake. The situation depicted in (A) is broadly equivalent to that shown in panels (C) and (D) in terms of stage of kame belt evolution. (B) Ice sheet with major subglacial drainage axis and late-stage ice-walled lake forming. (C) Partial collapse of drainage axis into early-stage lake as glacier karst begins to develop. (D) Lake expansion as glacier karst evolves. (E) Late-stage lake infill and ice-walled lake plains.
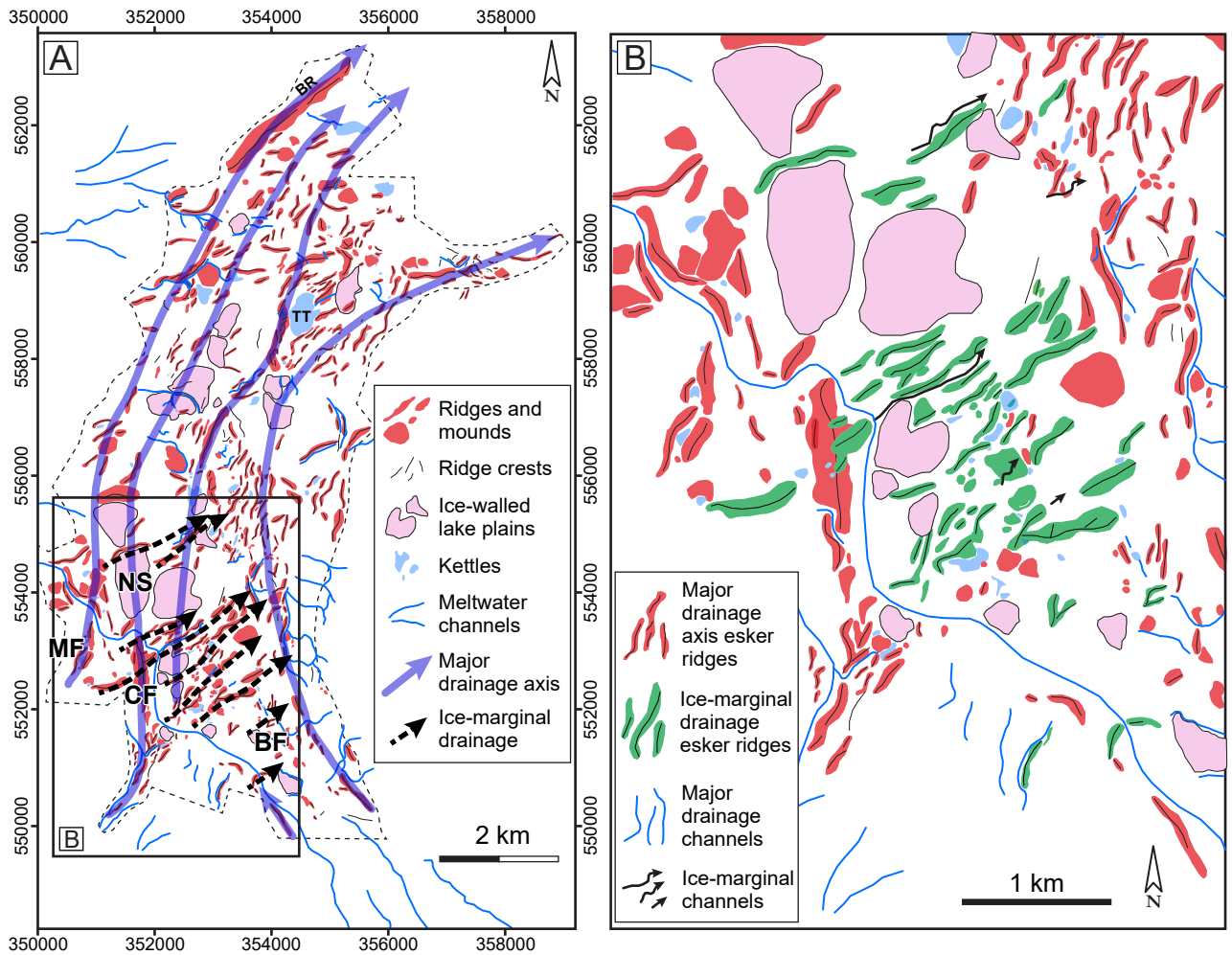
Figure 10 – Identification of two main styles of meltwater drainage within the Brampton Kame Belt. (A) Geomorphological map with identified major meltwater drainage axes oriented broadly S-N, and ice-marginal drainage routes aligned broadly SW-NE tracing ice sheet recession to the SE. (B) Southern part of the kame belt highlighting the difference between major drainage axis and ice-marginal drainage esker ridges.
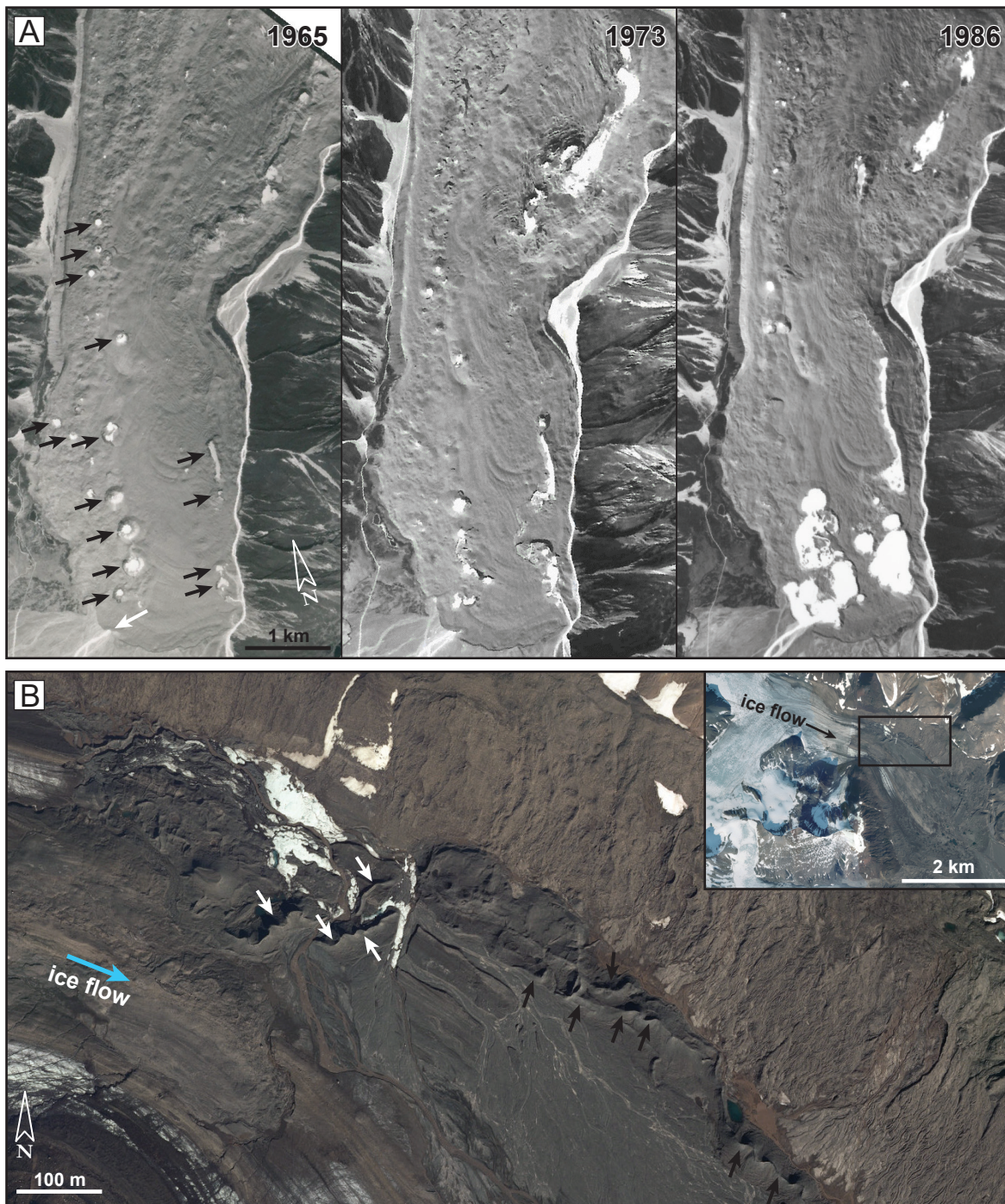
Figure 11 – Modern analogues for the two drainage network types identified within the Brampton Kame Belt. (A) Evolution from 1965 to 1986 of chains of supraglacial ponds (black arrows in left panel) on the debris-covered lower tongue of Tasman Glacier, New Zealand. Note that the axis of the chain of ponds coincides with the outflow of a subglacial channel (white arrow in left panel) at the glacier front. Aerial photographs from 1965, 1973 and 1986 are accessible from Land Information New Zealand (www.linz.govt.nz) and are used under the Creative Commons Attribution 4.0 International Licence. (B) Ice-marginal eskers (white arrows) at the margin of Hørbyebreen, Svalbard (see Storrar et al., in revision). Black arrows show flow-parallel eskers, analogous to the major drainage axis esker ridges in Fig. 10B. Inset shows context of the eskers at the glacier margin. Aerial photograph from 2009 acquired from the Norwegian Polar Institute TopoSvalbard online archive (toposvalbard.nploar.no).